Engineering Approaches for Improving Cortical Interfacing and Algorithms for the Evaluation of Treatment Resistant Epilepsy

by

Kari Rich Ashmont

A Dissertation Presented in Partial Fulfillment
of the Requirements for the Degree
Doctor of Philosophy

Approved November 2015 by the
Graduate Supervisory Committee:

Bradley Greger, Chair
Stephen Helms Tillery
Christopher Buneo
P David Adelson
F Edward Dudek

ARIZONA STATE UNIVERSITY

December 2015

ABSTRACT

Epilepsy is a group of disorders that cause seizures in approximately 2.2 million people in the United States. Over 30% of these patients have epilepsies that do not respond to treatment with anti-epileptic drugs. For this population, focal resection surgery could offer long-term seizure freedom. Surgery candidates undergo a myriad of tests and monitoring to determine where and when seizures occur. The "gold standard" method for focus identification involves the placement of electrocorticography (ECoG) grids in the sub-dural space, followed by continual monitoring and visual inspection of the patient's cortical activity. This process, however, is highly subjective and uses dated technology. Multiple studies were performed to investigate how the evaluation process could benefit from an algorithmic adjust using current ECoG technology, and how the use of new microECoG technology could further improve the process.

Computational algorithms can quickly and objectively find signal characteristics that may not be detectable with visual inspection, but many assume the data are stationary and/or linear, which biological data are not. An empirical mode decomposition (EMD) based algorithm was developed to detect potential seizures and tested on data collected from eight patients undergoing monitoring for focal resection surgery. EMD does not require linearity or stationarity and is data driven. The results suggest that a biological data driven algorithm could serve as a useful tool to objectively identify changes in cortical activity associated with seizures.

Next, the use of microECoG technology was investigated. Though both ECoG and microECoG grids are composed of electrodes resting on the surface of the cortex, changing the diameter of the electrodes creates non-trivial changes in the physics of the

electrode-tissue interface that need to be accounted for. Experimenting with different recording configurations showed that proper grounding, referencing, and amplification are critical to obtain high quality neural signals from microECoG grids.

Finally, the relationship between data collected from the cortical surface with micro and macro electrodes was studied. Simultaneous recordings of the two electrode types showed differences in power spectra that suggest the inclusion of activity, possibly from deep structures, by macroelectrodes that is not accessible by microelectrodes.

ACKNOWLEDGMENTS

To my advisor, Dr. Bradley Greger, I am not sure how to put my appreciation into words. You took a chance on me a few years ago and have supported me ever since. Under your guidance, I have grown and learned so much as a researcher and person. I hope one day I will have a fraction of your endless patience and optimism.

I would also like to thank the members of my committee for their mentorship. I owe particular thanks to Dr. Stephen Helms Tillery, who took me in as a naïve graduate student and is somehow still willing to talk, advise and collaborate with me.

I sincerely appreciate the clinicians, staff and patients at Phoenix Children's Hospital, particularly Dr. P. David Adelson, Yvette Sable and Danni Brown, who have helped me navigate the clinic world.

To of the lab-mates (and lab manager) I am fortunate enough to call friends, thank you for the therapeutic talks and comradery!

To my family, I know that my decision five years ago was a shock. Thank you for understanding when I did not call as often as I should or could not make the trip for the holidays. Your unwavering encouragement, advice, love and support mean everything.

Finally and most importantly, to my husband, Eric, who is undoubtedly my biggest supporter and best friend, and without whom I could not have made it through the past five years - thank you for keeping me grounded, for listening when I needed to talk, making me laugh when I needed to smile and always keeping me on my toes. Cheers to the close of this chapter and to the adventures that come next. We've got this.

TABLE OF CONTENTS

CHAPTER Page

CHAPTER Page

APPENDIX

LIST OF TABLES

Table Page

LIST OF FIGURES

Figure Page

CHAPTER 1

INTRODUCTION

Focal resection surgery can offer long-term control of seizures for people with treatment resistant epilepsy. Successful surgery relies on the accurate identification of where and when seizures originate. Currently, the identification process involves the sub-cranial implantation of large electrocorticography (ECoG) grids, followed by continual monitoring and visual inspection of cortical activity. Despite modern knowledge and technology that provide opportunities to improve the process, this "gold standard" method has remained largely unchanged since the technique was developed in the 1930's (Almeida, Martinez, & Feindel, 2005; Penfield, 1939; Tripathi et al., 2010).

The neocortex is arranged in a columnar structure. Cortical columns are 300-600 μm in diameter and are composed of heavily interconnected neurons running perpendicular to the cortical surface throughout the brain (Hubel, Wiesel, & Stryker, 1977; V. B. Mountcastle, 1997; V. Mountcastle, 1978). The individual neurons within cortical columns share common receptive fields and form small, functional units. Seizure activity has also been observed at spatial scales similar in size to a cortical column (Stead et al., 2010). Although ECoG offers better specificity than electroencephalography (EEG), standard clinical ECoG electrodes (diameter >1mm) are large and record signals from as much as 20 mm away (Menon et al., 1996). This size inconsistency means that a single ECoG electrode is recording from multiple cortical columns simultaneously, leading to spatial signal averaging and compromised specificity of the recordings. Identification accuracy is further complicated by the interpretation of cortical signals. An epileptologist reviews a patient's data and determines where and when a seizure occurs

based on visual inspection. This process is highly subjective. As data collection methods move towards improving specificity through increasing sampling frequencies and number of electrodes, these issues will continue to grow. Applying engineering concepts could help manage these concerns. To investigate this possibility, studies involving the recording and analysis of electrophysiological signals during the surgical evaluation process have been performed.

First, as described in Chapter 3, a computational algorithm based on empirical mode decomposition (EMD) that identifies changes in signal complexity was developed. EMD is a sifting algorithm that is data driven and does not rely on prior assumptions of linearity or stationarity. The sifting process produces intrinsic mode functions (IMFs), with the number of IMFs generated dependent on the complexity of the waveform. When EMD was windowed over the data, seizures were indicated by changes in the number of IMFs produced. A reliable computational method for detecting seizures could reduce the amount of time required to review a patient's data and will provide objective, repeatable results.

The EMD based algorithm was tested on seizure and non-seizure data clips from eight patients admitted to the pediatric epilepsy monitoring unit at Phoenix Children's Hospital (PCH) for pre-surgical monitoring of treatment resistant epilepsy. The algorithm identified seizures based on changes in signal complexity, but performed notably better on some patients than others. Specifically, when a patient's seizures originated from mesial structures, and subsequently localized to depth electrodes, the algorithm did not perform well.

Chapter 4 addresses the use of microelectrodes (diameter <1 mm) in cortical interfacing and the implications of reducing the electrode diameter. Critical aspects of the recording system, including electrode grid design, surgical placement, amplification, and recording are presented. By recording microelectrodes under different system configurations, the effects of poor grounding, referencing and amplification were tested.

The resulting signals and power spectra confirm that high quality signals can be recorded with microECoG grids. These signals, however, are vulnerable to noise and are easily contaminated if proper referencing, grounding, shielding and amplification are not performed.

The last study, presented in Chapter 5, aimed to investigate how signals are spatially averaged by macroelectrodes by trying to reconstruct a macroelectrode signal from 24 microelectrode signals surrounding it. To this end, a specialized electrode grid that combined micro and macro electrodes by surrounding individual macroelectrodes with consecutive circles of microelectrodes was designed and tested. All electrodes were recorded with the same system at a sampling frequency of 12.2 kHz for 10 minutes.

The custom grid was used to record from a patient with a cortical lesion immediately posterior to the central sulcus, undergoing surgical evaluation for treatment resistant epilepsy. Three groups of electrodes were simultaneously recorded; one of which was positioned over the cortical lesion. A spatially weighted contribution equation was developed to combine the microelectrode signals for comparison to the surrounding macroelectrode. Time and frequency analysis of the macroelectrode signals and the corresponding spatially weighted microelectrode signals showed moderate relationships. The correlation coefficient was lowest for the group of electrodes located over the

cortical lesion. Coherence values were higher in low frequency bands. Considering the larger volume of cortex from which macroelectrodes record signals, when compared to microelectrodes, the increased power likely arises from deep cortical structures. Additional data, ideally incorporating recordings from depth electrodes, could help to validate this concept.

Diagnoses have been based on visual inspection of recordings from large ECoG grids for decades without substantial change or improvement. Better sensitivity and specificity during the recording and analysis process is possible. The use of computational algorithms to aid in the data review process could serve as an objective point of standardization across centers while also reducing the amount of time spent reviewing data and revealing previously overlooked foci. This could lead to an increase in the number of patients deemed candidates for surgery and improve surgical outcomes. Further, the signals recorded with microelectrodes likely represent local synaptic activity and could fill a knowledge gap between single neuron activity recorded with penetrating electrodes and gross activity recorded with clinical ECoG in humans. This could help answer a variety of questions such as how interictal activity relates to seizure activity or how seizures manifest on a sub-millimeter scale (Staley, Hellier, & Dudek, 2005). Reducing the spatial averaging of signals could also lead to the identification of smaller epileptic foci and therefore smaller resection areas. Overall, any of these changes have the potential to improve patient care and could possibly lead to a better long-term quality of life.

CHAPTER 2

BACKGROUND

Epilepsy

Epilepsy refers to a continuum of neurological disorders that cause an increased likelihood of seizures that affects men and women of all ages. A person is said to have epilepsy when he or she has at least one seizure (Fisher et al., 2005). It is estimated that 1 in 26 people in the United States will be diagnosed with epilepsy at some point in their lifetime (England, Liverman, Schultz, & Strawbridge, 2012). That means that, at any one time, there are approximately 2.2 million people in the United States living with epilepsy (England et al., 2012). There are multiple types of epilepsy with many different causes that result in a variety of seizures.

Etiologies. More than 25 etiologies are associated with epilepsy and are separated into three general groups; genetic, structural and metabolic, and unknown causes (Berg et al., 2010; England et al., 2012).

Genetic. Genetic epilepsies are caused by a defect at either the chromosomal or molecular level, but are not necessarily inherited (Berg et al., 2010). Most genetic epilepsies are caused by mutations that affect the production of protein used in ion channels but others can cause issues with structural development of the brain (Abad, Sanmartí Vilaplana, & Serratosa, 2007).

Structural and metabolic. Structural abnormalities can be acquired through stroke, traumatic brain injury or infection, or caused by genetic and developmental issues. Epilepsy caused by infection of the central nervous system are especially prevalent in developing countries. Common seizure-causing infections include bacterial meningitis,

viral encephalitis, cerebral malaria, tuberculosis, HIV, neurocysticercosis and cerebral toxoplasmosis.

Cases of lesional epilepsy are also considered structural and metabolic. The most common of which is hippocampal sclerosis, a developmental abnormality. Others include tubular sclerosis and hypothalamic hamartomas. A patient with a structural abnormality is 1.5 times more likely to have seizures that cannot be controlled with anti-epileptic drugs (AEDs) than patients with other etiologies (P Kwan & Brodie, 2000). However, the presence of a structural abnormality improves the chance of seizure freedom from resection surgery.

Metabolic issues can disrupt the brain's energy metabolism, electrolytes, osmolality, or acid-base balance and cause seizure activity. Metabolic epilepsies could also impact the way anti-epileptic drugs are processed which could lead to further complications (O'Brien, 1998).

Unknown. Unknown epilepsies was previously referred to as "cryptogenetic". As many as one-third of all epilepsy cases have causes that are unknown.

Seizures. A seizure is considered an abnormal, synchronous firing of a group of neurons in the brain. Seizures fall into one of two categories; generalized or partial.

Generalized. Generalized seizures are those that have sudden, bilateral involvement of either cortical or subcortical structures in the brain (Berg et al., 2010). There are several types of generalized seizures. Clonic seizures have rapid contraction and relaxation of muscles. Tonic seizures cause a significant increase in muscle tone, while convulsive, or tonic-clonic seizures involve both presentations; stiffening of muscles (tonic) and abrupt, jerking movements caused by the contraction and relaxation

of muscles (clonic). Atonic seizures or "drop seizures" cause sudden loss of muscle tone. Finally, myoclonic seizures involve sudden, brief jerks that are more localized than those associated with clonic seizures. Finally, absence seizures are generally associated with an altered state of awareness where the patient may stare blankly into space.

Partial/Focal. Unlike generalized seizures, partial seizures are localized to one area, though they may spread. Simple partial seizures involve activity that originates from a focal area in one hemisphere of the brain during which consciousness is not affected. If the simple seizure spreads, it is considered secondarily generalized. A complex partial seizure also starts in a localized area but does impact the patient's consciousness.

Unclassified. Some seizure manifestations, such as certain neonatal seizures, do not fall into the categories listed above and are there for considered part of an unclassified group. Seizures may be unclassified due to insufficient knowledge or data (Penry, 1981).

Status epilepticus. The length and severity of a seizure can vary. Most seizures do not last more than two minutes (Dobesberger et al., 2015; Shinnar, Berg, Moshe, & Shinnar, 2001). If a patient has a seizure lasting more than five minutes or multiple occurring in such rapid succession that normal consciousness is not regained between seizures, the patient is said to be in status epilepticus (Penry, 1981). Status epilepticus is dangerous and is associated with increased incidence of permanent brain damage and sometimes death. When available, medical intervention in the form of anti-epileptic drugs (AEDs) is used to interrupt status epilepticus.

Treatments.

Anti-epileptic drugs. The most common form of treatment for epilepsy is anti-epileptic drugs (AEDs). There are approximately 26 AEDs available with modes of action including membrane stabilization, reduction of neurotransmitter release or increasing GABA-mediated inhibition (Howard et al., 2011). The correlation between mode of action and resulting clinical activity is not completely understood and many AEDs have secondary actions and side effects. Monotherapy is generally advised, though combination therapy may be beneficial for some patients (Howard et al., 2011).

Treatment resistant epilepsy. Although doctors are able to control many patients' seizures with AEDs, over one third of patients with epilepsy are treatment resistant (P Kwan & Brodie, 2000). For these patients, other options need to be considered. Treatment resistant epilepsy, also referred to as refractory or drug-resistant epilepsy, is considered the failure to gain control of seizures after two appropriately prescribed AED trials of adequate length (Patrick Kwan et al., 2010). The chances of a patient gaining control of seizures from a third AED, if they have already failed to respond to two others, is between 1% and 3% (P Kwan & Brodie, 2000).

Dietary regimes. Common dietary plans include the ketogenic, modified Atkins and low glycemic index diets. The ketogenic diet has been used since the 1920's and involves a high fat, low carbohydrate diet and is meant to mimic fasting. The exact therapeutic mechanism of the ketogenic diet is not known, but is thought to involve the increase of ketones in the body or the stabilization of blood sugar. The ketogenic diet is effective for a range of treatment-resistant epilepsies, with more than 50% of patients on the diet experiencing greater than 50% reduction in seizures, but is difficult to maintain

and has side effects (Lefevre & Aronson, 2000). Other dietary plans include the modified Atkins diet, which is less restrictive but still causes ketosis and the low glycemic index diet, which targets blood sugar stabilization (Kossoff et al., 2006; Muzykewicz et al., 2009).

Surgery. Surgery is an option that can offer long-term control of seizures in patients with treatment resistant epilepsy. There are two types of surgical approaches for treating epilepsy; resection and disconnection.

Resection surgery involves removing the seizure focus, i.e. the area of the brain from which seizures originate and is particularly successful for those who have mesial temporal epilepsy with hippocampal sclerosis, a hypothalamic hamartoma with gelastic seizures, hemiconvulsion and hemiplegia, or Rasmussen syndrome (Berg et al., 2010).

Disconnection surgery was introduced in 1961 and is an alternative to resection surgery when seizures occur in areas of eloquent cortex, where removing tissue could have a detrimental impact on the patient's daily life (Geschwind & Kaplan, 1962). The goal of disconnection surgery is to break the pathway of activity associated with seizures such that the extent of spread is limited. Modern disconnection surgery includes multiple subpial transection (MST), corpus callosotomy (CCS) and modified functional hemispherectomy (DFH) (Shimizu & Maehara, 2000).

Surgical evaluation. Surgical candidates undergo a series of tests and procedures to determine where the seizures are coming from and the likely-hood of seizure freedom from surgery. This process is broken down into two phases; Phase I and Phase II.

Phase I evaluation typically includes anatomical and functional imaging such as CT, PET and MRI scans, neuropsychology evaluation and video electroencephalography

(EEG) monitoring to get information on the patient's general brain function, and to lateralize and locate seizure foci (Cross et al., 2006). While EEG has the benefit of being non-invasive, the epi-cranial placement of the electrodes significantly distorts waveforms and often prevents precise localization of seizure onset. The information gained does, however, provide information to help epileptologists determine candidacy for Phase II evaluation and to identify a general area of seizure onset to target for electrode placement during Phase II tests.

In the event that the EEG and imaging data are discordant or more information is needed, the patient is referred for Phase II evaluation. In Phase II, subdural electrocorticography (ECoG) grids and/or depth electrodes, for certain deep foci, are placed in the region of the brain thought to be the seizure onset zone. After the initial surgery, the patient will enter the Epilepsy Monitoring Unit (EMU) where cortical activity and video will continuously be recorded. The monitoring period serves two purposes; identifying where and when seizures originate and determining how the foci are positioned with respect to other cortical structures. These objectives are accomplished through continual recording of cortical activity and mapping via bipolar stimulation of electrodes. In order to proceed with the surgical resection, the clinical team needs to be confident that the patient has focal seizures that do not occur in areas of eloquent cortex (Snead III, 2001). That is, that removing that area of the brain will not impact critical daily functions such as moving or speaking, and that the patient will be seizure-free after the resection. If a patient's seizures are coming from eloquent cortex, i.e. an area of the brain needed for critical daily functions such as speech or movement, the patient may not be a surgical candidate.

Surgical outcomes. Outcomes of resection surgeries vary and depend on a number of factors that could include the extent of resection and the presence of particular pathologies. Between 54.7% and 79.4% of patients are seizure free in the first two years post-surgery, but the chance of continued seizure freedom 10 years after resection surgery drops to only 33% (Spencer, et al., 2005; Bulacio, et al., 2012). Disconnection surgery is less likely to provide seizure freedom than resection surgery. Patients who undergo disconnection surgery do, however, show variable levels of improvement of cognitive function and speech, with notable decreases in the number of drop attacks suffered (Shimizu & Maehara, 2000).

Neuromodulation. Neuromodulation refers to the attempt to alter the endogenous function of an individual neuron or a group of neurons. This is often done by inducing electrical stimulation. Neuromodulation methods to treat epilepsy include deep brain stimulation (DBS), vagus nerve stimulation (VNS), and responsive stimulation.

Deep brain stimulation. DBS uses long depth electrodes to target subcortical structures and periodically emit an electrical pulse. Though the precise mechanistic underpinnings of DBS is not fully understood, stimulation seems to disrupt or block unregulated activity associated with seizures (Halpern, Samadani, Litt, Jaggi, & Baltuch, 2008). Structures targeted by DBS include the thalamus, subthalamic nucleus, cerebellum, hippocampus, caudate nucleus and mammillary nuclei (Halpern et al., 2008). Results of DBS vary depending on the structure stimulated and seem to improve with time. Dramatic improvements reported are approximately 93% reduction in seizure frequency (Halpern et al., 2008).

Vagus nerve stimulation. The vagus nerve is a large nerve that transports signals between the chest and stomach and the brain. VNS involves the implantation of a programmable stimulation device that sends electrical shocks to the vagus nerve. Approximately 35% of patients respond (> 50% seizure reduction) and very few (3.4%) see full control (>90% seizure reduction) of their seizures (Galbarriatu et al., 2015).

Responsive stimulation. Responsive stimulation is a closed-loop approach to using electrical stimulation to modulate seizure activity. ECoG electrodes are placed over the seizure focus and records activity and a stimulating depth electrode emits a pulse when the activity is thought to be associated with the patient's seizures, based on a detection algorithm. Devices can be adjusted by physicians as needed for optimal control of seizures. Patients reported between 35% and 43% decreases in frequency and severity of seizures while using the responsive stimulation therapy (F.T., M.J., & R.E., 2008).

Biological Signals: Composition, Scale and Characteristics

Cortical layers. The neocortex is horizontally divided into six layers, each with their own cytoarchitecture. The thickness of the cortex itself varies in different areas of the brain, but is about 2.3 mm on average. Layer I is sparsely populated with cell bodies and consists mainly of axonal and dendritic terminations, and primarily functions as a hub for connections between distal dendrites and cortical and thalamic inputs (Douglas & Martin, 2004; Ray, Crone, Niebur, Franaszczuk, & Hsiao, 2008). Layers II and III are frequently grouped together and also receive some subcortical inputs. Layer II consists of densely packed granule cells and layer III is predominately pyramidal cells. Together, they receive sensory and motor inputs from other parts of the cortex. Layer IV is a thin layer consisting of stellate and granule cells that receive inputs from the thalamus and

project to layers II/III (Miller, Pinto, & Simons, 2001; Ray et al., 2008). Layer V is primarily pyramidal cells with non-pyramidal cells sparsely present that largely receive cortico-cortical inputs and project to various subcortical structures. Layer VI is mostly closely packed spindle-shaped cells interspersed with fiber bundles with some pyramidal cells that take part in thalamic and reciprocal cortico-cortical interactions (Thomson & Lamy, 2007).

Cortical columns. Cortical columns consist of many chains of heavily interconnected neurons that run vertically through layers II-VI of the neocortex (V. B. Mountcastle, 1997; V. Mountcastle, 1978). Each chain contains all major cortical neural cell types and are bound to other chains via short, horizontal connections (V. B. Mountcastle, 1997; V. Mountcastle, 1978). Cortical columns are between 300 and 600 μm in diameter and act as small, computational units that transmit and receive information (V. B. Mountcastle, 1997; V. Mountcastle, 1978).

Local field potentials. Local field potentials (LFP) are multi-unit neural signals that are composed of all ionic processes in an area of the brain (Buzsáki, Anastassiou, & Koch, 2012). The spatial and temporal extent of LFPs is debated. LFP oscillations occur over the course of seconds and generally between 1 and 300 Hz (Buzsáki et al., 2012; Schendel et al., 2013). Although some studies indicate an LFP spatial resolution in the millimeter range, others have suggested areas as small as 250 micrometers (Kajikawa & Schoeder, 2012).

The precise biophysics and neural circuitry underlying the generation of LFPs is still not fully understood, but they likely arise from many signal generators of various shapes, sizes and locations, and propagate through the brain by some combination of

volume conduction, ephaptic, and synaptic mechanisms (Anastassiou, Perin, Markram, & Koch, 2011; Hales & Pockett, 2014). Regardless of the underlying mechanisms, it is clear that LFPs carry substantial information related to cortical processes such as movement and speech, and likely pathologies such as epilepsy (S. S. Kellis, House, Thomson, Brown, & Greger, 2009; S. Kellis et al., 2015; Leuthardt, Freudenberg, Bundy, & Roland, 2009; Stead et al., 2010)

Electrocorticography

Electrocorticography (ECoG) is a method of measuring electrical signals of the brain using surgically placed sub-cranial grids and strips. Surface ECoG measures the difference between electric currents released by dipoles in the brain and a ground, or reference electrode (Buzsáki et al., 2012).

Geometry. ECoG grids consist of platinum-iridium or stainless steel wires that terminate to discs in silicon bedding. Dimensions of clinical ECoG grids vary. Common layouts include 64 electrodes arranged in an 8x8 square or 20 electrodes in a 4x5 rectangle. Strips may have a 1x4 or 1x6 electrode arrangement. Typical electrodes in grids and strips are between 4 and 5 mm in diameter, with an exposed contact diameter of 2 to 3 mm and 10 mm between electrodes, center to center. Reference and ground electrodes are usually not included in a clinical electrode grid, and are separate, abbreviated strips.

Depth electrodes are long, needle like probes that penetrate the cortex and are used to record from deep structures suspected of contributing to seizure activity. A typical depth electrode consists of a 1.3 mm diameter polyurethane shaft with four, six or eight platinum/iridium contacts 2.3 mm long space 5 or 10 mm apart, center to center.

Placement. ECoG electrodes are surgically implanted below the skull via a large craniotomy (Hill et al., 2012). Grids and strips can be placed epi-durally, though sub-dural placement is more common as the dura decreases signal quality. This placement reduces their vulnerability to movement artifacts and increases the spatial resolution compared to EEG, while their estimated duration of functional life and stability is increased compared to penetrating electrodes, which initiate a complicated foreign body response (S. S. Kellis et al., 2009; Schalk & Leuthardt, 2011). Following placement, the dura and skull flaps are re-positioned and the recording tails are brought through the skin, creating small trans-cutaneous holes.

Depth electrodes are stereotactically inserted perpendicular to the cortical surface into medial structures such as the amygdala and hippocampus. Similar to surface grids, the recording tails of the depth electrodes are brought through the skin for percutaneous connection.

Recording. ECoG, as it is used in clinical applications such as epilepsy monitoring, is a multi-unit recording method with signals as high as 100 μm and is typically sampled at 250 or 500 Hz, though research applications may use higher rates. Clinical ECoG cannot differentiate signals produced by individual neurons. Waveforms recorded with ECoG represent general fluctuations in the spatial and temporal summation of ionic processes generated by a group of active neurons in the same area (Buzsáki et al., 2012). The precise composition of the dipoles recorded by ECoG electrodes is debated but seems to depend on the type, density, orientation, size and synaptic organization of neurons within the electrode's recording radius (Ray et al., 2008). A significant component of ECoG signals is likely activity from pyramidal cells in layer V of the

cortex. Pyramidal cells have extensive dendritic arborization, including apical dendrites that run in parallel for relatively long distances, thus increasing the chance of obtaining the spatial and temporal summation needed to generate a signal large enough to be recorded by an ECoG electrode (Ferree, Clay, & Tucker, 2001).

Engineering Approaches

Diagnoses have been based on visual inspection of recordings from large ECoG grids for decades without substantial change or improvement. Better sensitivity and specificity during the recording and analysis process is possible.

Mathematical approaches to detecting seizures. Computational algorithms may be able to improve the sensitivity and specificity of seizure detection. Further, they could objectively identify where and when a seizure starts on a smaller spatial and temporal scale than visual inspection (Lehmkuhle et al., 2009; Lodder & van Putten, 2013). Despite a number of attempts and reasonable accuracy of some of the computational algorithms developed, visual inspection has remained the method of choice for epileptologists (Lodder & van Putten, 2013). This could be due to a variety of reasons. The time-varying dynamics of neural signals and high levels of inter and intra patient variability make quantification and detection of seizures difficult (Haas, Frei, & Osorio, 2007). Many of the algorithms used assume that the signal is stationary and/or linear and are therefore ill-suited for and cannot fully describe the complexity of the biological signals they are meant to analyze (Lehnertz, 2008; Oweis & Abdulhay, 2011). That is, the algorithms assume that the signal's parameters, such as variance or standard deviation, will not change over time and that a constant slope will be maintained. Others require *a priori* knowledge of the signal to correctly choose the most appropriate inputs for the

algorithm or assume that the signal is composed of specific waveforms such as sinusoids or particular wavelet functions. A clinically useful algorithm will be robust enough to work well on all variations of biological signals that may be associated with seizure and non-seizure activity, without *a priori* knowledge about the signal or assumptions that the signals are stationary or linear.

Fourier Transform. The Fourier transform breaks a signal into its component frequencies. It assumes that the original signal is linear, stationary, and composed of sinusoids (Fourier, 1822). One of the first attempts to mathematically detect seizures was based on the relatively simple Fast Fourier Transform (FFT) and used phase and coherence calculations to find small time differences between waveforms on different channels (Gotman, 1983). Though it was originally thought the patient's seizures were generalized, the time differences found suggested the presence of an epileptic focus (Gotman, 1983). Though the Fourier transform is a useful tool in many aspects, biological signals, such as ECoG data, is not linear, stationary, or composed of sinusoids. Thus, the use of FFT for the analysis of biological data is not ideal.

Wavelets. Similar to the Fourier transform, the wavelet transform assumes the signal is composed of specific elements (Haar, 1911). Wavelet transforms decompose signals into components based on how well they match a pre-selected wavelet function, referred to as the "mother wavelet". While the mother wavelet can be scaled in amplitude and frequency to better capture the shape of the waveform being analyzed, the user must know what the signal looks like in order to choose the correct mother wavelet. The wavelet transformation has been used as the basis for many seizure detection algorithms

(Fathima, Bedeeuzzaman, Farooq, & Khan, 2011; Rosso, Blanco, & Rabinowicz, 2003; Samar, Bopardikar, Rao, & Swartz, 1999; Schiff, 1994). Similar to the Fourier transform, the wavelet transform is a useful tool, but is not well suited for the analysis of biological data.

Empirical mode decomposition (EMD). Empirical mode decomposition (EMD) is an adaptive sifting algorithm that iteratively breaks down complex waveforms into simpler, component waveforms. EMD does not require the prior assumption of stationarity or linearity of the signal and is fully data driven, making it well suited for the analysis of biological data (N. E. Huang et al., 1998; Norden E Huang, 2005). EMD breaks down a signal into intrinsic mode functions (IMF) which are modes of oscillation whose number of zero crossings and extrema differ at most by one and whose envelope mean crosses zero at some point (N. E. Huang et al., 1998). IMFs have variable amplitude and frequency with respect to time and the final number of IMFs depends on the complexity of the original signal. The ability of the EMD algorithm to detect a seizure is based on changes in the complexity of cortical activity, with regard to amplitude and frequency, during a seizure when compared to a non-seizure state.

Microelectrocorticography. Similar to ECoG, micro-electrocorticography (microECoG) grids are composed of electrodes that measure differences between dipoles in the brain and a reference electrode. The size of the electrodes (diameter <1 mm) and subsequently the number of dipoles recorded by an individual electrode, however, is significantly smaller than that of a clinical ECoG grid electrode. Each microelectrode records from a cortical volume on the sub-millimeter scale (Schalk & Leuthardt, 2011). At this scale, microECoG can record "local field potential-like" signals produced by time

evolving ionic activity in small neuronal populations, and individual cortical columns or neurons (S. S. Kellis et al., 2009; Khodagholy et al., 2014). This means that, compared to clinical ECoG, the specificity of the recordings is improved because there is less spatial averaging and the sensitivity is increased because fewer ionic processes are superimposed to produce the signal recorded. It has been shown that microECoG arrays do improve recording specificity by offering better spatial resolution than clinical ECoG grids (S. S. Kellis et al., 2009).

Geometry. MicroECoG grids are frequently custom designs. Microelectrodes are sub-millimeter in diameter and are either placed in the interelectrode space of a clinical grid or arranged in a manner to study a particular question of interest. Due to their high impedance and small recording area, the interelectrode spacing is typically much smaller than that of clinical ECoG grids. Interelectrode spacing of 1 mm produces an approximate 90% correlation between neighboring electrodes, though large interelectrode spacing could allow activity to go undetected (S. S. Kellis et al., 2009; C. a. Schevon et al., 2009).

Placement. Like clinical ECoG, microECoG grids are placed below the skull, but do not penetrate the cortical surface. Most often, microelectrodes are either added to the inter-electrode spacing of a clinical ECoG grid, or positioned into a separate stand-alone grid. The small form factor of microelectrodes and grids typically allow their placement within the margins of the craniotomy performed for clinical purposes. Microelectrodes that are to be placed underneath the intact bone flap are more difficult due to the protrusion of the microelectrodes from the silicon bedding, towards the surface of the brain. In these situations, the electrodes are placed through a combination of strategies

including slight retraction of the brain as well as copious irrigation underneath the grid/microelectrode to "float" the electrodes in place.

Recording. Though similar to clinical ECoG in many aspects, microelectrodes have significantly higher impedance. Impedance is the resistance created by a circuit when a current is applied to it and changes based on the frequency of the signal being generated. The change in impedance affects many aspects of the recording system used and the signals it records. High resistance at the electrode-tissue interface means that the recording radius of a microelectrode is significantly smaller than that of a clinical ECoG electrode, which is low impedance. A smaller recording radius indicates less spatial summation of neuronal activity taking place and therefore smaller signal amplitudes recorded that are highly susceptible to noise contamination. To mitigate noise issues, proper referencing, grounding, shielding and head-stage level amplification are needed.

Microelectrodes record surface LFPs and possibly APs, both of which have broad and likely over lapping temporal scales (Khodagholy et al., 2014). To ensure high fidelity and avoid aliasing of signals, microECoG is typically recorded at a higher frequency than clinical ECoG; multiple kilohertz.

CHAPTER 3

AN ALGORITHMIC ADJUNCT TO VISUAL INSPECTION: USING EMPIRICAL MODE DECOMPOSITION TO DETECT SEIZURES

Introduction

It is estimated that 1 in 26 people in the United States will be diagnosed with epilepsy at some point in their lifetime (England et al., 2012). Although many patients' seizures can be controlled with anti-epileptic drugs, estimates suggest that 22.5% of patients with epilepsy are drug-resistant (Patrick Kwan, Schachter, & Brodie, 2011). For these patients, epilepsy surgery utilizing either focal resection or neuromodulation may be an effective treatment. Surgical candidates undergo a series of tests and procedures, typically including anatomical and functional imaging and video electroencephalography (EEG) monitoring to lateralize and locate a seizure focus. In the event that the data is discordant, surface electrocorticography (ECoG) grids or depth electrodes for certain deep foci are placed in the region of the brain thought to be the seizure onset zone. The current "gold-standard" for the evaluation of a patient's cortical activity is visual inspection by an epileptologist. This process is time consuming, subjective and lacks specificity and sensitivity (Binder & Haut, 2013). The use of a computational algorithm to help with the evaluation process could mitigate some of these concerns.

The inherent subjectivity in the interpretation of EEG signals has been acknowledged for over 50 years, yet little has been achieved to improve the process (Gerber et al., 2008; Houfek & Ellingson, 1959). High levels of inter and intra-rater variability are confounded by a lack of standardization in the evaluation process across centers (Gerber et al., 2008). While standardizing terminology and training programs

may be difficult to establish, using a computational algorithm as a point of standardization for the evaluation procedures would have the added benefit of producing objective, quantitative results that could be compared across centers (Lehmkuhle et al., 2009; Lodder & van Putten, 2013).

Surgical outcomes vary and seem to depend on a number of factors such as the extent of resection and the presence of particular pathologies, i.e. hippocampal sclerosis, tumors, etc. (Bergen, 2006). Patients have between a 54.7% to 79.4% chance of seizure freedom for 2 years following surgery (Bergen, 2006). The chance of continued seizure freedom drops significantly, to 33%, at 10 years post-resection (Bulacio et al., 2012). The continuation or reoccurrence of seizures following resection surgery is generally attributed to incomplete resection of the epileptic focus, the development of new, second foci, or some underlying epileptogenic network that is not yet understood (Bergen, 2006; Bulacio et al., 2012). All of which indicate outcomes can be improved.

There may be a micro-scale epileptogenic environment that relates to seizure generation and propagation which cannot be detected with standard clinical electrodes (C. a. Schevon et al., 2009; Stead et al., 2010; Worrell et al., 2008). Recording micro-scale activity with the same coverage as clinical ECoG grids would require many microelectrodes, different equipment, and higher sampling rates than what are used in clinical recordings today. Though this would improve the sensitivity and specificity of recordings, it would also significantly increase the amount of data that needs to be reviewed and therefore the time it takes for epileptologists to review it. Even with today's recording technology, computational algorithms may detect subtleties that cannot be seen in visual inspection (Gotman, 1983; Lodder & van Putten, 2013; Schindler,

Leung, Elger, & Lehnertz, 2007). Considering the improvements to electrophysiologic technology, it is easy to appreciate that computational algorithms may be useful now, but will become more standard in the future.

Computational algorithms have seen some success in assessing seizure activity, but none have been adopted into the clinical evaluation process. Many studies focus on the prediction of seizure events using complex mathematics (Aschenbrenner-Scheibe et al., 2003; Iasemidis, 2003; Mormann, Andrzejak, Elger, & Lehnertz, 2007; Pardalos et al., 2004). It is worth noting that the goal of this work, however, is not to predict, but rather to detect seizure events. One of the first attempts to detect seizures by quantifying differences in seizure and non-seizure data was based on the relatively simple Fast Fourier Transforms (FFT) and used phase and coherence calculations to detect small time differences between waveforms on different channels (Gotman, 1983). The related wavelet transformation, which attempts to match recorded signals with a pre-selected wavelet function, has been used as the basis for many seizure detection algorithms. Results from one analysis using changes in power paired with wavelet analysis reports 100% sensitivity and specificity but was limited to recordings from depth electrodes only from patients with mesial temporal foci (Osorio, Frei, & Wilkinson, 1998). Other wavelet methods reported sensitivities ranging from 64% to 88%, depending on the wavelet function used (Gutiérrez, Alcántara, & Medina, 2001).

These frequency and power based algorithms, however, are not designed for use on biological signals. Biological signals, especially those involved with seizure events, have highly complex dynamics and are neither linear nor stationary (Bergey & Franaszczuk, 2001; Lodder & van Putten, 2013). Yet, many mathematical algorithms

used to analyze biological signals, such as FFT and wavelet transforms, assume that the signal is linear and/or stationary and that the signals are composed of specific elements; sinusoids and wavelet functions, respectively (Fourier, 1822; Haar, 1911; Norden E Huang, 2005). A clinically useful algorithm will be robust enough to work well on all variations of biological signals that may be associated with seizure and non-seizure activity, without *a priori* knowledge about the signal or assumptions that the signals are stationary or linear.

Unlike other algorithms, EMD is data driven and does not rely on *a priori* assumptions of linearity or stationarity; i.e. EMD does not assume that the signal maintains a constant slope or the same mean and variance over time (N. E. Huang et al., 1998; Norden E Huang, 2005). Recognition that its attributes make EMD well suited for the analysis of biological signals has led to its use in seizure detection algorithms (Bizopoulos, Tsalikakis, Tzallas, Koutsouris, & Fotiadis, 2013; Li, Zhou, Yuan, Geng, & Cai, 2013; Orosco, Laciar, Correa, Torres, & Graffigna, 2009; Pachori & Bajaj, 2011). One study using EMD and higher order statistics reported 56.41% sensitivity and 75.86% specificity while another paired EMD with machine learning and achieved 100% specificity and sensitivity (Alam & Bhuiyan, 2013; Orosco et al., 2009).

Previous studies used EMD as a pre-processing tool where EMD breaks down a signal into multiple component signals, which are then manipulated with complex analyses. Here, it was noted that the number of resulting component signals is a measure of how complex the original signal is and that signal complexity changes during seizures (Bergey & Franaszczuk, 2001). By applying EMD iteratively to each data clip and counting the number of component signals produced, changes in the signal complexity

associated with seizure activity are tracked over time without the need for sophisticated calculations. Though the algorithm presented here is highly iterative, it is mathematically simple. It is hypothesized that this EMD based algorithm could serve as an early screening method for seizure detection and facilitate confirmatory clinical observations.

Materials and Methods

Patients. The Phoenix Children's Hospital and Arizona State University Institutional Review Boards approved this study, with a waiver of consent. All data and information were collected after the patient left the hospital and was de-identified prior to use.

ECoG data from eight patients admitted to the pediatric epilepsy monitoring unit (PEMU) at Phoenix Children's Hospital (PCH) (Phoenix, AZ, USA) were collected. The placement of subdural grids and subsequent monitoring was performed as standard of care for Phase II evaluation of children with treatment resistant epilepsy to localize a seizure focus and determine the suitability for respective surgery. The data were recorded with an XLTEK EMU128FS (Natus Medical Incorporated, San Carlos, CA, USA) at a sampling frequency of 500 Hz. The data were visually reviewed and annotated to identify seizure onset times and locations by epileptologists, per clinical standard of care.

Datasets. The recorded data were broken down into 136 ten-minute long clips. There were 68 seizure clips that were centered on a clinically determined seizure onset times, and 68 associated non-seizure clips. To avoid biasing the data towards a particular patient, no more than 15 seizure clips were extracted for each patient. For all but 12 seizures, the non-seizure data clips were taken 40-30 minutes prior to each seizure onset

time. In these 12 instances, because data 40-30 minutes prior to the seizure were not available, the non-seizure clips were extracted from non-seizure time epochs as allowed by the data recordings.

Analysis. All analyses were performed using MATLAB (MathWorks Incorporated, Natick, MA, USA). Prior to applying EMD, the signals for each grid were common average re-referenced (CAR) (Ludwig et al., 2009).

Empirical mode decomposition. Empirical mode decomposition (EMD is an algorithm that was developed to iteratively decompose complex waveforms into intrinsic mode functions (IMF). IMFs are oscillatory signals with variable amplitude and frequency as functions of time (Norden E Huang, 2005). EMD is data driven and will continue to decompose the signal into IMFs until the signal becomes monotonic or falls below a user-defined threshold. Therefore, the number of IMFs produced by EMD depends on the amount of complexity with respect to frequency and amplitude in the signal. EMD assumes that the data consist of at least one maximum and one minimum, the characteristic time scale is defined by the time difference between the extrema and that if the data lack extrema, differentiation could reveal maxima and minima (N. E. Huang et al., 1998). EMD is typically applied in conjunction with the Hilbert Spectral Analysis in the Hilbert-Huang Transform (HHT) and is used to study nonlinear and nonstationary wave dynamics. EMD is well qualified for the analysis of biological data because it does not require stationarity or linearity of the signal, is data driven and does not assume that the signal consists of defined components such as sinusoids or wavelets, and does not need prior knowledge of the signal (Fourier, 1822; Haar, 1911; Norden E Huang, 2005).

To begin the decomposition process, local maxima and local minima are connected with two cubic spline interpolations to generate maxima and minima envelopes of the primary data, $x_i(t)$. The mean of these envelopes, $\boldsymbol{m}_j$, is then calculated and subtracted from the primary data (Figure 3.1).

$$\boldsymbol{h}_j = x_i(t) - \boldsymbol{m}_j \tag{3.1}$$

The resulting vector, $\boldsymbol{h}_j$, represents the first potential IMF of the decomposition process. $\boldsymbol{h}_j$ is considered an IMF if :

(1) The number of extrema and zero crossings in $\boldsymbol{h}_j$ differ at most by one

(2) The mean of the envelopes of $\boldsymbol{h}_j$ is zero at any point.

If $\boldsymbol{h}_j$ does not meet the IMF criteria above, $\boldsymbol{h}_j$ is re-processed until it becomes an IMF.

$$\boldsymbol{h}_j = \boldsymbol{h}_{(j-1)} - \boldsymbol{m}_j \tag{3.2}$$

where $j = j + 1$, or six consecutive iterations occur in which $\boldsymbol{h}_j$has the same number of zero crossings and extrema, and the two values differ at most by one for six consecutive iterations. Then,

$$\boldsymbol{IMF}_k = \boldsymbol{h}_j \tag{3.3}$$

where $k = 1, 2 \ldots .$ $\boldsymbol{IMF}_k$ is then subtracted from the primary data leaving residual data,

$$R_m(t) = x_i(t) - \boldsymbol{IMF}_k \tag{3.4}$$

The decomposition is considered complete when the residual, $R_m(t)$, is "less than the predetermined value of substantial consequence" or becomes monotonic (Norden E Huang, 2005). If the residual data exceeds this value of substantial consequence, the

residual data becomes the primary data and is reintroduced into the beginning of the EMD process (Figure 3.1 D).

$$x_{i+1}(t) = R_m(t) \tag{3.5}$$

For this analysis, the process was stopped when the residual fell below a mean peak-to-peak amplitude of 20 μV or a frequency of 2 Hz. These stopping criteria were used to ensure that biological data above the noise floor of the amplifier was being analyzed.

Seizure detection. EMD was applied to each data clip and each electrode separately. EMD analysis was performed using a sliding window of 5 s in length, with a step size of 3 s. The number of IMFs resulting from EMD in each 5 s window was then tabulated to produce a time evolving IMF trace for each electrode (Figure 3.1 C). Two thresholds were established, one for each individual electrode and one for the population of all electrodes (Figure 3.1 C & D). Electrographic events were identified by considering changes in the number of IMFs generated for each individual electrode. Potential seizures were marked based on patterns in increases in the number of IMFs across the population of all electrodes in a given clip**.**

To determine an individual electrode threshold, the mean and mode of the number of IMFs per 5 s window were calculated. The larger of the two measures served as a threshold. Next, windows that contained more IMFs than the threshold were found. When a number of IMFs per window was greater than the threshold, persisted for at least four consecutive windows (14 s) and occurred fewer than 40 times (2 mins and 2 s) in the data clip, an electrographic event was marked for that electrode. If a particular number of IMFs per window was greater than the threshold, but occurred more than 40 times during the 10 min clip, it was considered part of the general activity recorded and became the

new threshold for that electrode instead of an electrographic event. The onset time of an electrographic event on an electrode was noted as the median time of the first of the four consecutive windows containing the elevated number of IMFs. Electrographic events that occurred more than 1 min apart were considered separate events.

An electrographic event on a single electrode is unlikely to represent seizure activity. Therefore temporal clustering of electrographic events across many electrodes was used to detect potential seizure activity. If the number of electrodes on which electrographic events occurred within 30 s of each other exceeded the population threshold of seven, then a potential seizure was considered detected. The middle of the 30 s window in which the threshold was crossed was marked as the potential seizure onset time. A population threshold of seven was used after multiple numbers were tested during the development of the algorithm as an informal optimization method. Onsets separated by more than 5 min were considered to be separate potential seizure detections.

Seizure times used were taken from notes made by the epileptologist during the visual review process, without a prompt to mark precise onset times. Therefore, a broad timeframe of +/-5 min of the seizure time noted was used to classify potential seizure onsets as detected by the EMD based algorithm as true positives. Potential seizures detected by the EMD algorithm in non-seizure clips were considered false positives. When multiple potential seizures were detected in a clip by the EMD based algorithm, the clip was labeled a true positive and the potential seizure onset time closest to the clinically determined onset time was used in the remainder of the analyses.

Statistical analysis. The two-sample Kolmogorov-Smirnov (KS) test was used to demonstrate that there was a significant difference between the number of IMFs that occurred during a potential seizure and the number of IMFs that occurred during non-seizure activity for the same patient. The comparison was made between 2 mins of data from seizure and non-seizure clips from the same patient. The 2 mins of data from seizure clips began at the potential seizure onset time and was averaged across the electrodes involved in the seizure for that clip. Non-seizure data were taken from the center of each non-seizure clip and averaged across all electrodes.

To determine the performance of EMD at seizure detection, sensitivity and specificity calculations were performed based on the true positive and false negative labeling of each clip. Rates were determined on a patient-by-patient and overall patient population basis.

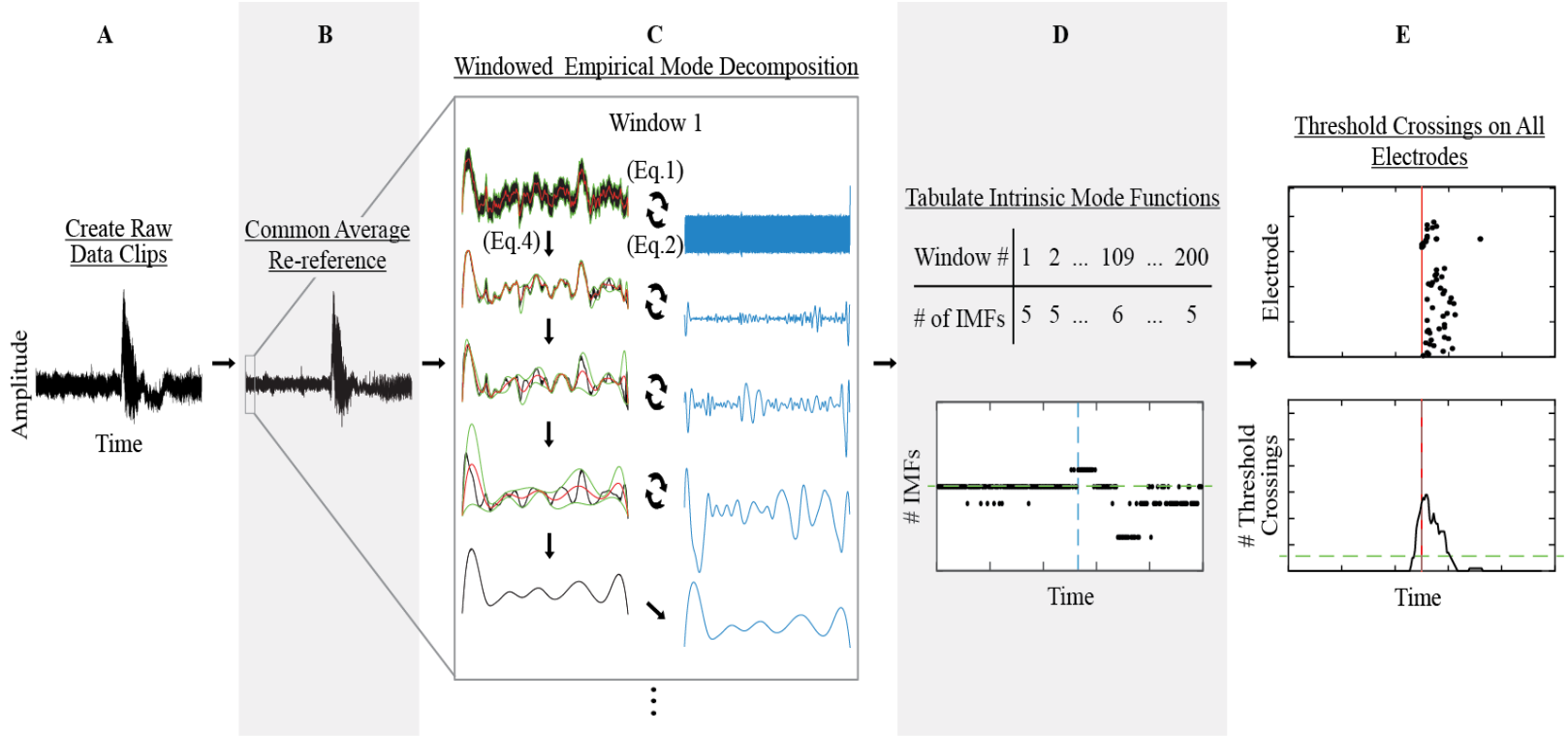
A
Create Raw Data Clips
Amplitude
Time
B
Common Average Re-reference
C
Windowed Empirical Mode Decomposition
Window 1
(Eq.1)
(Eq.2)
(Eq.4)
D
Tabulate Intrinsic Mode Functions
Window # 1 2 ... 109 ... 200
# of IMFs 5 5 ... 6 ... 5
IMFs
Time
E
Threshold Crossings on All Electrodes
Electrode
Threshold Crossings
Time

Figure 3.1. Algorithm flow diagram. A graphical representation of the windowed EMD algorithm and thresholds. The raw data that is broken down into 10 min clips, then denoised using common average re-referencing. EMD is then applied to a 5 s window of data $x_i(t)$ (black). Maximum and minimum envelopes (green) and the mean of the envelopes $\boldsymbol{m}_j$ (red) are calculated, then the average (red) is subtracted from the data (black). If the difference $\boldsymbol{h}_j$ (blue) meets the criteria of an IMF, it is then subtracted from the original data (black) leaving residual data. If the difference does not result in an IMF, the difference is enveloped and the process repeats until an IMF is created (process not show in figure). The residual data is then set as the data (Equation 3.5) and the decomposition proceeds. The process continues until the average peak to peak amplitude of the residual data falls below 20 mV or the average frequency is below 2 Hz. The number of IMFs produced from EMD are then tabulated to determine the individual electrode threshold (green dashed line). Finally, threshold crossings on all electrodes within a 10 min data clip are evaluated. When seven or more population threshold crossings occur within the same 30 s, a potential electrographic event onset (blue dashed line) is marked as the middle of that 30 s window.

Results

Data from eight patients with varying ages, grid locations and etiologies when undergoing ECoG monitoring for treatment resistant epilepsy were collected. Table 1 summarizes the clinical data pertaining to the patients. For all tables and figures, patients highlighted in grey had seizure onset zones localized to depth electrodes by the reviewing epileptologist.

Table 3.1
Patient Information

Patient # (age-gender)	Pathology	Implant Location	Seizure Onset Zone
1 14 years female	Dysembryoblastic Neuroepithelial Tumor & Focal Cortical Dysplasia Palmini Type IIIB	*Surface:* Left posterior temporal with occipital and parietal coverage *Depth:* Sub-temporal	Left temporal
2 15 years male	Focal Cortical Dysplasia Palmini Type IIA	*Surface:* Interhemispheric fissure (double-sided), left occipital, superior parietal and lateral temporal	Left/midline occipital
3 17 years male	Focal Cortical Dysplasia Palmini Type IIA	*Surface:* Interhemispheric fissure (double-sided), left convexity (front and temporal) *Depth:* Mesial Frontal	Left hemispheric (depth electrode)
4 14 years male	No resection	*Surface:* Left angular gyrus, orbitofrontal and sub-temporal *Depth:* Insular regions	Left posterior insula/post-central gyrus (depth electrode)
5 20 years male	Ammon's Horn Sclerosis	*Surface:* Left convexity (frontal and temporal), temporal (anterior, mid and posterior) and superior frontal	Left mesial temporal
6 2 years male	Low-Grade Glioma & Focal Cortical Dysplasia Palmini Type IIIB	*Surface:* Centered on left Sylvian fissure, sub-temporal *Depth:* Mesial temporal	Multifocal in left hemisphere (depth electrode)
7 9 years male	Focal Cortical Dysplasia Palmini Type IIA	*Surface:* Right temporal, sub-temporal and orbitofrontal *Depth:* Insular regions and hippocampus	Right sub-temporal and some lateral temporal
8 14 years male	Focal Cortical Dysplasia Palmini Type IIIB	*Surface:* Interhemispheric fissure, left central cortex *Depth:* Mesial left central	High left central midline (depth electrode)

The EMD based algorithm was able to detect events on individual electrodes from seizure clips from each patient, despite variations in electrographic morphology (Figure 3.2).

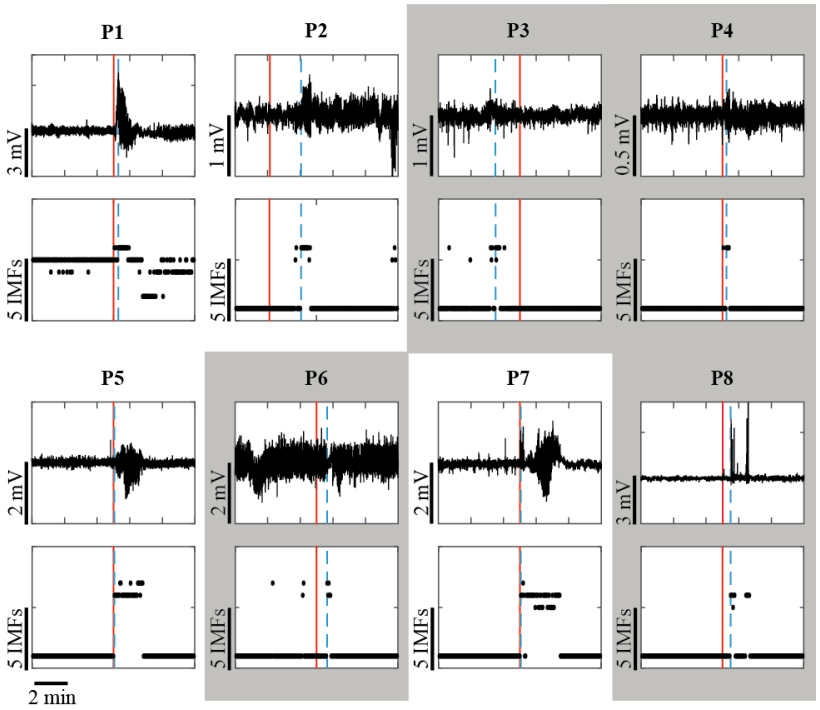

Figure 3.2. Electrographic data and IMFs resulting from windowed EMD of seizure clips. Examples of single electrode electrographic data and the number of IMFs resulting from EMD on seizure clips from each patient. The solid red line marks the seizure onset time noted by the reviewing epileptologist. The dashed blue line marks the onset of the electrographic event as detected with EMD. Patients highlighted in grey had clinically determined seizure onset zones localized to depth electrodes.

A total of 2064 electrographic events were detected on the 787 electrodes used to record from the eight patients studied during the 68 seizure clips (Table 3.2).

Table 3.2

EMD Threshold Results from Seizure Clips

			Electrographic Events			Potential Seizures		
Patient	**Electrodes**	**Seizure Clips**	**Total**	**Mean Abs Offset (s)**	**Offset SD (s)**	**Total**	**Mean Abs Offset (s)**	**Offset SD (s)**
P1	98	5	228	70.17	21.41	5	9.60	6.50
P2	118	3	95	80.77	52.12	3	87.00	81.00
P3	120	6	206	67.46	56.42	6	120.50	57.47
P4	94	10	111	66.73	59.20	4	5.25	1.50
P5	89	13	517	53.88	57.41	13	25.38	24.05
P6	88	10	299	70.61	61.23	6	61.50	30.99
P7	90	15	476	98.72	23.97	14	18.00	12.17
P8	90	6	132	67.75	34.20	3	20.00	4.58

*SD = standard deviation; Abs = absolute value

Fewer (n = 784) electrographic events detected in the 68 non-seizure clips (Figure 3.3 and Table 3.3). A breakdown of the events detected per patient during seizure clips and how they related to clinical marks is given in Table 3.2. The mean number of electrographic events detected per seizure clip ranged from 11.1 for Patient 4 to 45.6 for Patient 1 (Figure 3.4). The mean of the absolute values of all offset times between the clinically determined seizure onset time and the time of electrographic events detected

was 72.93 s SD ± 44.92 s (Table 3.2). The mean of the absolute values of the time differences between potential seizures detected with EMD and the clinically noted onset time was 43.34 s SD ± 27.28 s (Table 3.2). Of the 54 potential seizures detected by EMD in seizure clips, 19 were detected before the clinically noted seizure onset time.

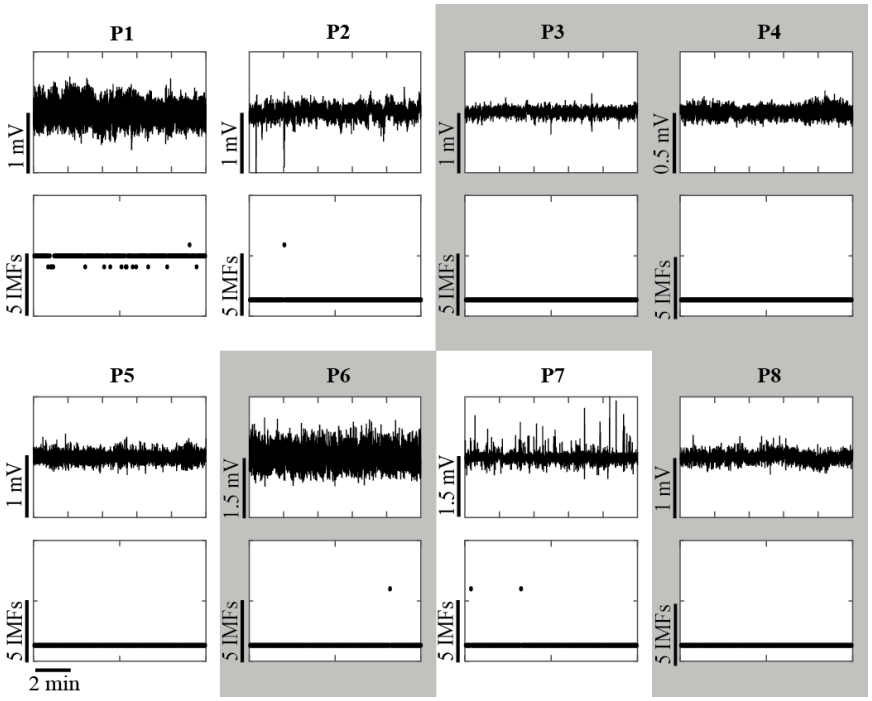

Figure 3.3. Electrographic data and IMFs resulting from windowed EMD of non-seizure clips. Examples of single electrode electrographic data and the number of IMFs resulting from EMD on non-seizure clips from each patient. Patients highlighted in grey had clinically determined seizure onset zones localized to depth electrodes.

Table 3.3

EMD Threshold Results from Non-Seizure Clips

Patient	Electrodes	Non-Seizure Clips	Total Electrographic Events	Total Potential Onsets
P1	98	5	28	0
P2	118	3	55	2
P3	120	6	103	4
P4	94	10	32	0
P5	89	13	108	2
P6	88	10	103	5
P7	90	15	257	6
P8	90	6	30	0

Most (91.13%) of the electrographic events detected were on surface electrodes. Of the 787 electrodes used to record from the eight patients studied, 96 (12.2%) were depth electrodes, yet only 8.87% of the 2064 electrographic events detected were on depth electrodes. There were no potential seizure onsets detected by the EMD based algorithm that only included electrographic events detected on depth electrodes. Clinically determined mesial onsets accounted for 12 of the 14 false negative classifications. There were a total of 45 seizures analyzed that were localized to surface electrodes by the epileptologists. The EMD based algorithm detected 95.56% of these seizures. The algorithm detected 52.17% of seizures localized to depth electrodes. Seizure onsets localized to surface electrodes by visual inspection gave a more

pronounced detection result by the EMD based algorithm than seizures with clinically determined mesial onsets (Figure 3.4 and 3.5).

Potential seizure onsets were found in 54 of the 68 seizure clips analyzed, resulting in an EMD sensitivity of 79.41%. Of the 14 false negative clips (seizure clips in which the EMD based algorithm failed to detect a seizure detected by the epileptologist), 12 clips contained data from seizures for which the epileptologist listed depth electrodes as the onset location. Potential seizures were detected in 14 of the 68 non-seizure clips by the EMD based algorithm. The overall specificity of the EMD based algorithm was 79.41%, with a mean false positive rate of 1.24 FP/hr. Examples of non-seizure results can be found in the (Figure 3.6 and 3.7). The patient-by-patient specificity and sensitivity information is shown in Table 3.4. With the exception of the 14 seizure clips in which the EMD based algorithm failed to detect a seizure, the number of IMFs per window associated with the potential seizures was significantly different from the number of IMFs per window from non-seizure activity (Table 3.4).

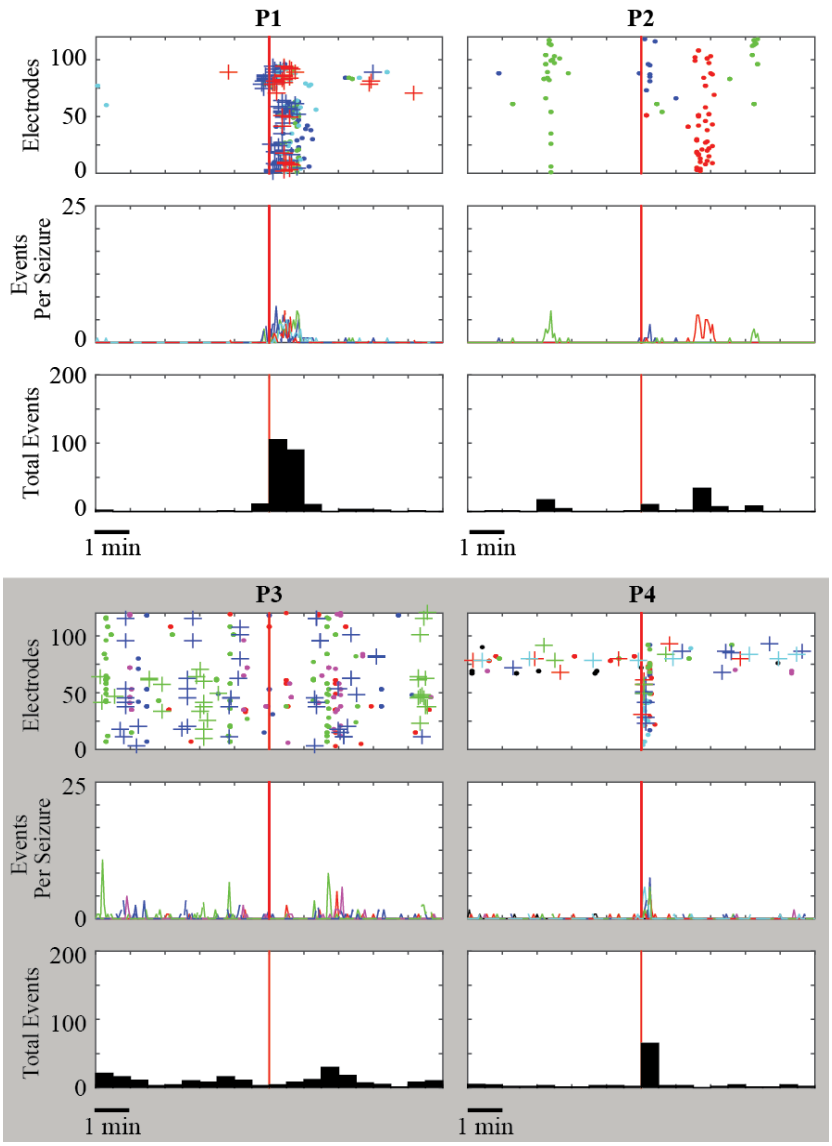

Figure 3.4. Electrode threshold crossings in all seizure clips from P1, P2, P3, and P4. Electrode threshold crossings were more common on surface electrodes compared to depth electrodes. All threshold crossings for all patients (n = 8) during all seizure clips analyzed (n = 68) are shown relative to the clinically determined onset time, denoted by the red vertical line. The different symbols and line types correspond with the different seizure clips. The seizure onset zone was localized to depth electrodes for P3 and P4.

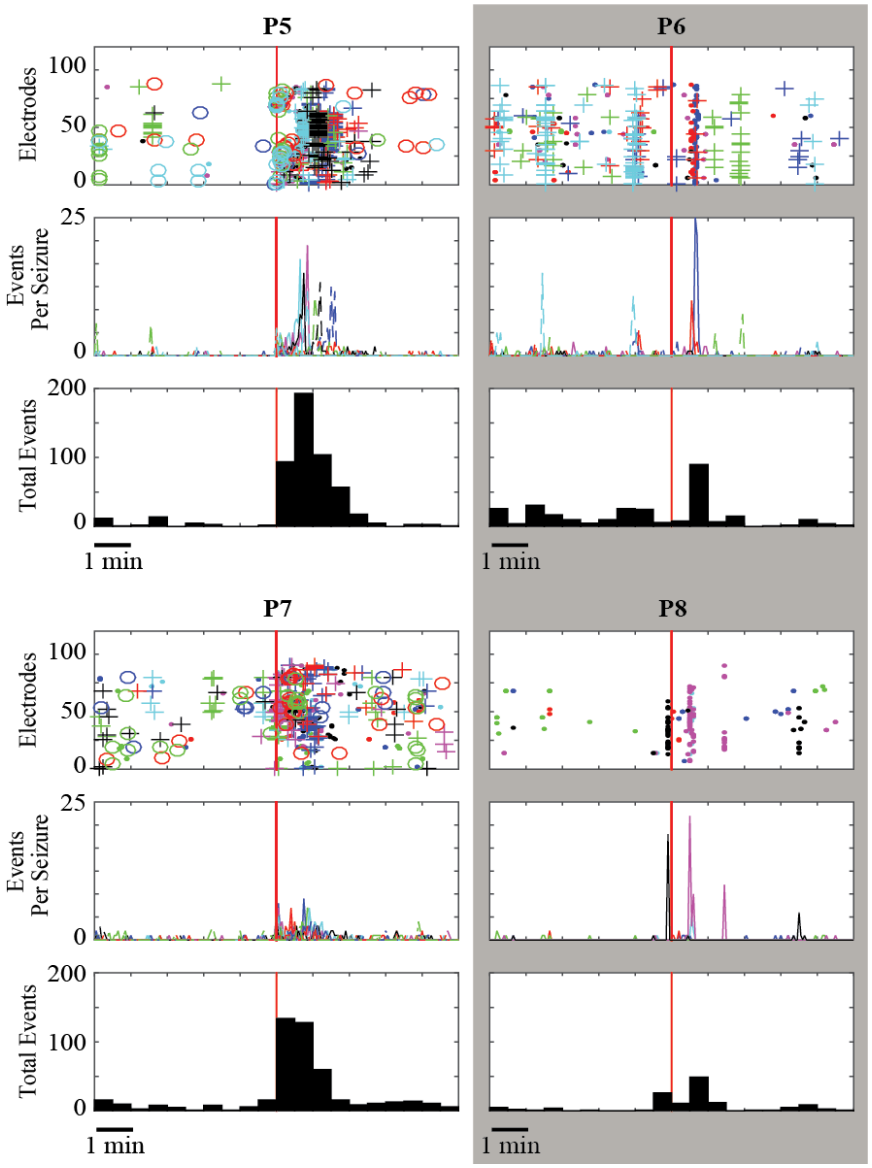

Figure 3.5. Electrode threshold crossings in all seizure clips form P5, P6, P7, and P8. Electrode threshold crossings were more common on surface electrodes compared to depth electrodes. All threshold crossings for all patients (n = 8) during all seizure clips analyzed (n = 68) are shown relative to the clinically determined onset time, denoted by the red vertical line. The different symbols and line types correspond with the different seizure clips. The seizure onset zone was localized to depth electrodes for P6 and P8.

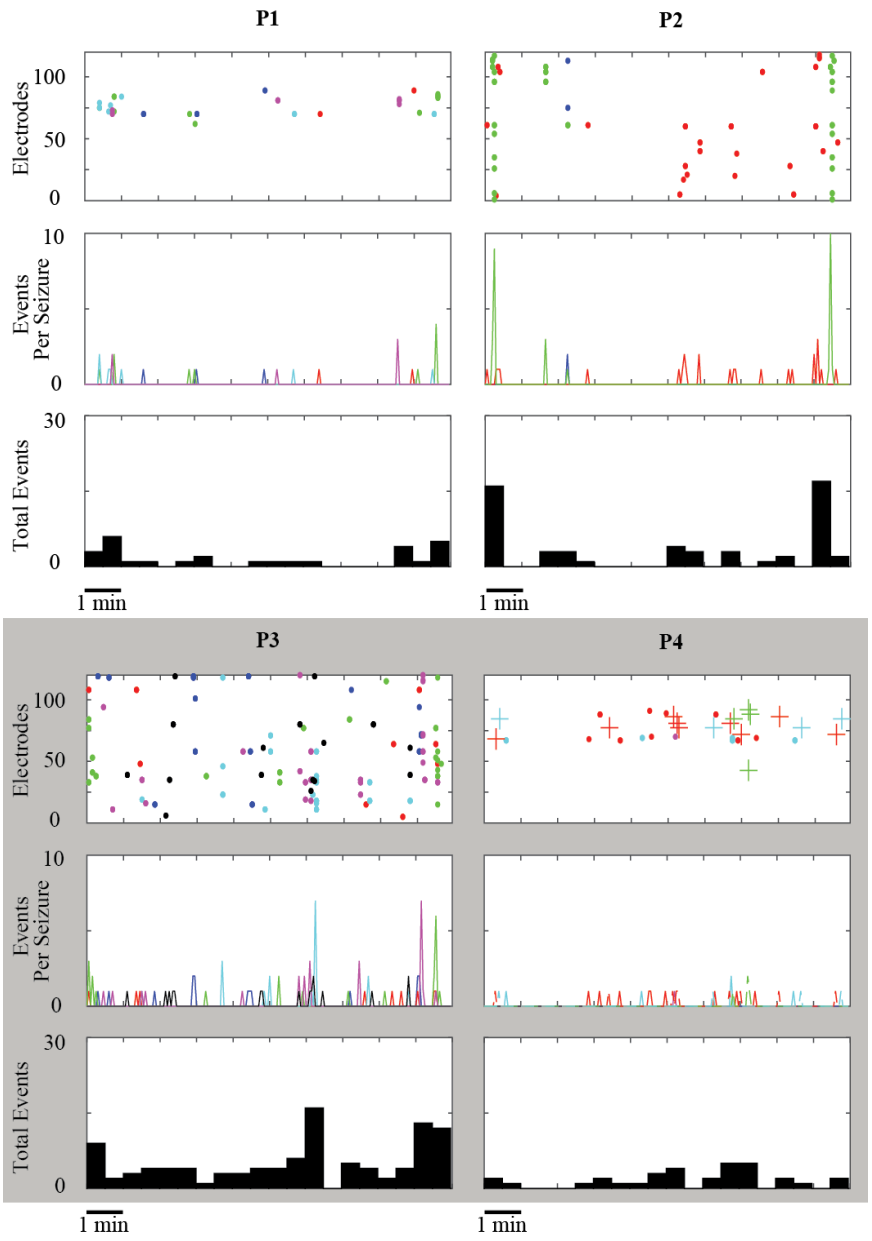

Figure 3.6. Electrode threshold crossings in all non-seizure clips from P1, P2, P3, and P4. All threshold crossings for each patient during all (n = 68) non-seizure clips (designated by the different symbols) analyzed are shown. P3 and P4 had seizures that were localized to depth electrodes by the reviewing epileptologist.

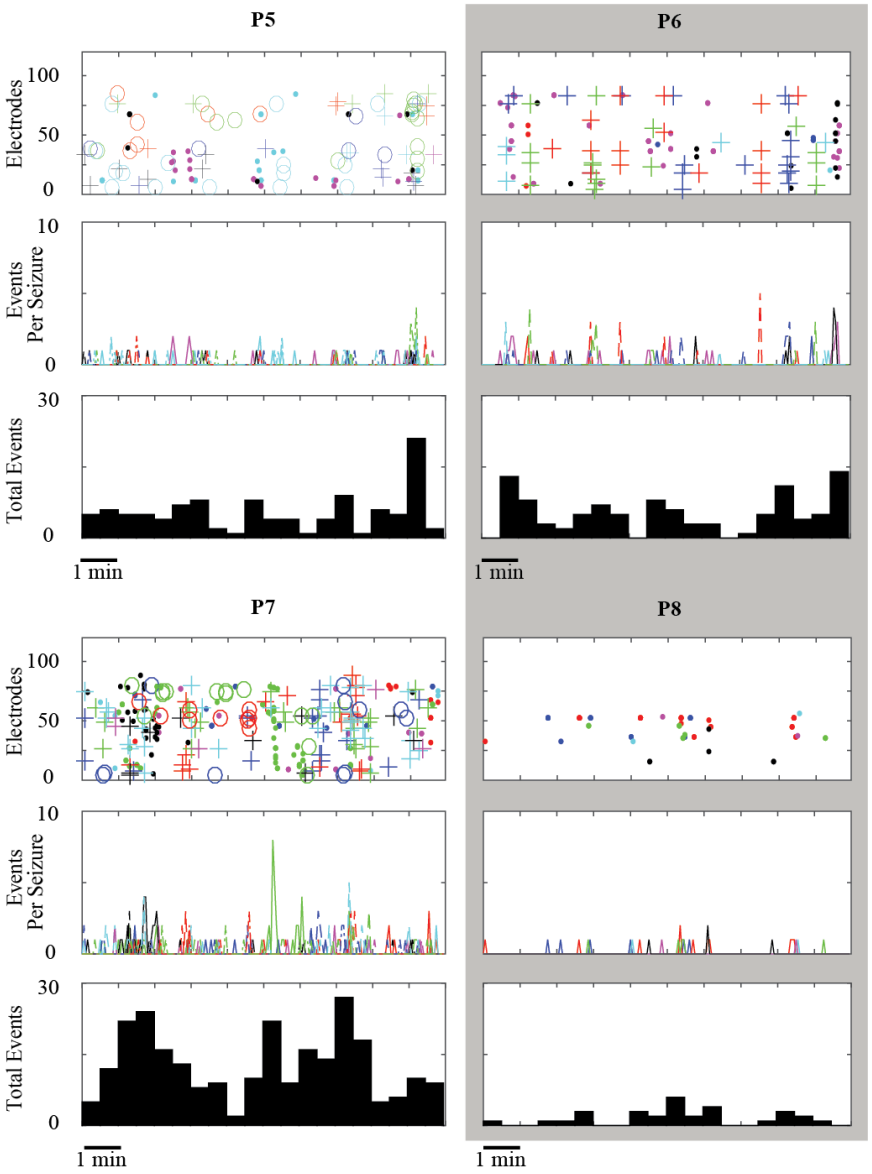

Figure 3.7. Electrode threshold crossings in all non-seizure clips from P5, P6, P7, and P8. All threshold crossings for each patient during all (n = 68) non-seizure clips (designated by the different symbols) analyzed are shown. P6 and P8 had seizures that were localized to depth electrodes by the reviewing epileptologist.

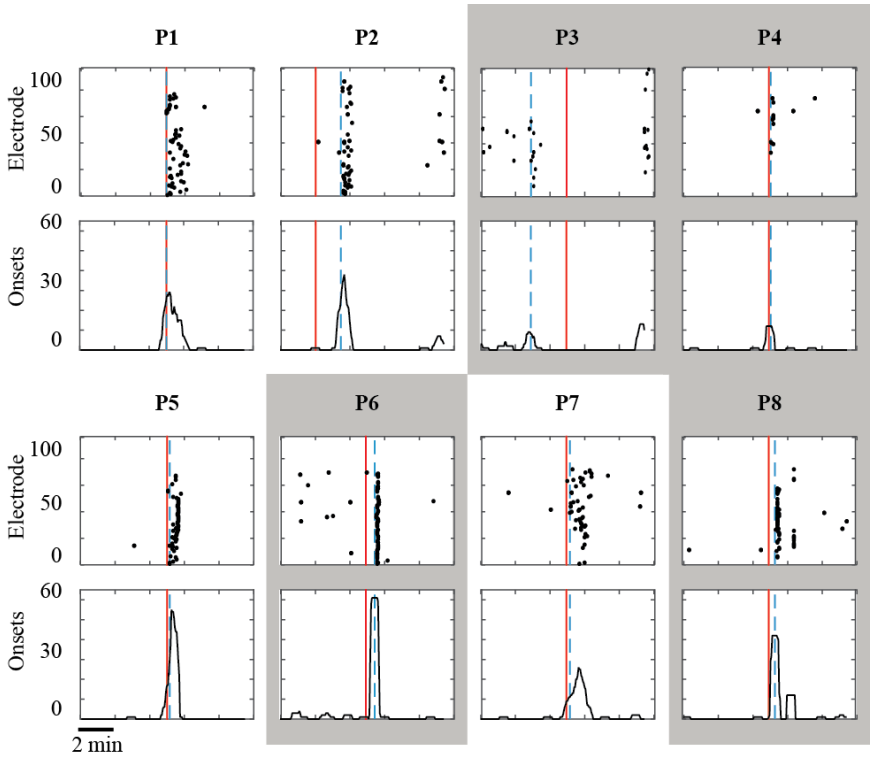

Figure 3.8. Population thresholds of single seizure clips. EMD detected onsets across all electrodes and the resulting population threshold to find seizure candidates. The solid red line marks the seizure onset time noted by the reviewing epileptologist. The dashed blue line marks the EMD detected seizure onset time which is considered when the number of IMFs per window is greater than the individual electrode threshold on at least seven electrodes in the same 30 s period. Patients highlighted in grey had clinically determined seizure onset zones localized to depth electrodes.

EMD performed better on data from some patients than others. This was apparent at the population level (Table 3.2) as well as the electrographic event level (Figure 3.8). The mean number of electrographic events per seizure clip ranged from 11.1 for P4 to 45.6 for P1. This matched the order of sensitivity levels of EMD at seizure detection (a result

of the population threshold), with P4 having the lowest mean sensitivity of 40.00% and P1 having 100.00% (Table 3.4).

Table 3.4

EMD Seizure Detection

Patient	Seizure Clips	TP	FN	Non-Seizure Clips	FP	TN	Sensitivity (%)	Specificity (%)	Mean P-Value
P1	5	5	0	5	0	5	100.00	100.00	$1.40x10^{-6}$
P2	3	3	0	3	1	2	100.00	67.00	$7.08x10^{-6}$
P3	6	6	0	6	3	3	100.00	50.00	$1.07x10^{-5}$
P4	10	4	6	10	0	10	40.00	100.00	$1.88x10^{-14}$
P5	13	13	0	13	1	12	100.00	92.00	$8.94x10^{-5}$
P6	10	6	4	10	3	7	60.00	70.00	$2.21x10^{-4}$
P7	15	14	1	15	6	9	93.00	60.00	$3.23x10^{-5}$
P8	6	3	3	6	0	6	50.00	100.00	$3.97x10^{-8}$

TP = true positive; FN = false negative; FP = false positive; TN = true negative

The mean number of IMFs per window that occurred in electrographic events involved with a potential seizure detected in a seizure clip was compared to the mean number of IMFs across all electrodes in non-seizure clips. For all true-positive seizure detections (n=54 out of 68), the differences in the comparisons were significant for all seizure clips, at a 99.5% confidence level.

Discussion

Algorithms for biological signals. The findings demonstrate that an EMD based algorithm could be used as a seizure detection tool. Unlike other algorithms, the method

presented here is data driven, does not require that the signal is linear or stationary, does not need *a priori* knowledge of the signal and is mathematically simple. Though EMD does assume that the signal consists of oscillatory modes, i.e. waveforms that satisfy the criteria of an IMF, this is a less strict assumption than Fourier transforms assuming a signal consists of sinusoids and wavelet transforms assuming the signal contains a specific wavelet waveform. Using an EMD based algorithm to mark potential seizures prior to the visual review process may reduce the amount of data an epileptologist needs to review and therefore the amount of time spent reviewing those data. Further, the potential seizures would objectively and quantitatively be identified. This could help to decrease the amount of intra- and inter-rater variability and to standardize the review process by providing data that could easily be compared across centers (Binder & Haut, 2013; Gerber et al., 2008). Beyond the PEMU, this sort of algorithm could be even more useful in the evaluation of critically ill patients undergoing monitoring in the intensive care unit, where non-convulsive seizures are common and immediate treatment is critical (Gerber et al., 2008).

Differences between the clinically noted seizure times and the start of potential seizures detected by the EMD based algorithm had high standard deviations. This likely reflects multiple sources of variance. The EMD based detection algorithm has its own inherent variance as do each of the reviewing epileptologists. Additionally, the reviewing epileptologists were not requested to mark the precise beginning of seizures, and may have been marking times that reflect a general timeframe of interest before or during the seizure.

When compared to seizure onsets detected with visual inspection, the EMD based algorithm was able to detect clinically marked seizures that were not obvious from electrocorticography data (Figure 3.2). It also found potential seizures in non-seizure data (Figure 3.9 and 3.10). While some false positive detections appear to be due to general noise that happened to temporally align, others have compelling electrographic waveforms that suggest seizure activity that was not marked during visual inspection (Figure 3.10). These false-positive detections may have been missed, but could also be a result of the patient having highly stereotyped seizures in which case the epileptologist reviewed all seizures but stopped marking them after they had sufficient data to base a diagnosis.

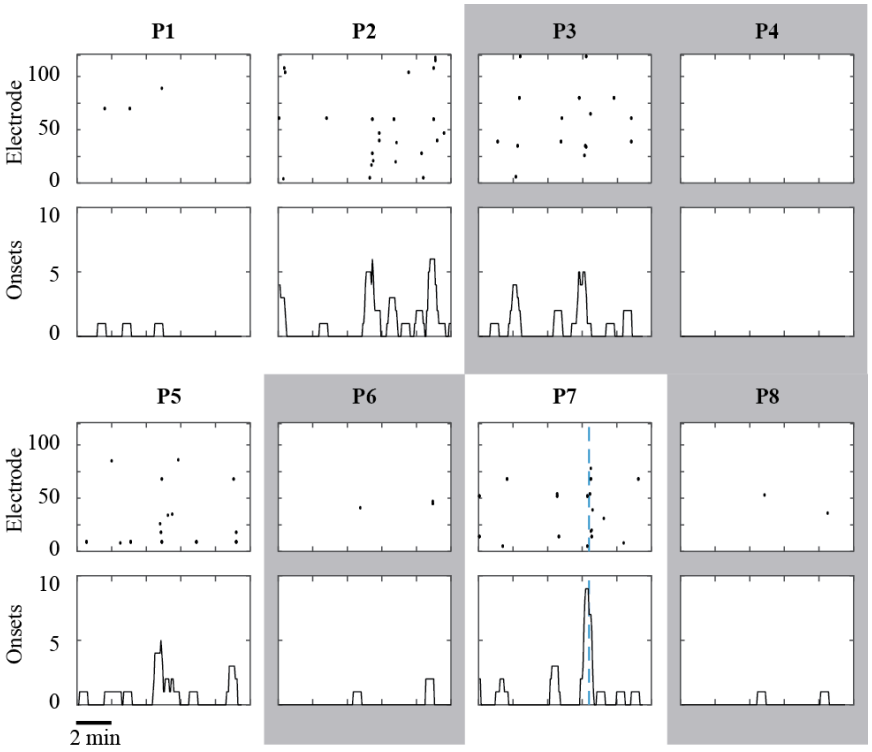

Figure 3.9. Population thresholds of single non-seizure clips. EMD detected onsets across all electrodes and the resulting population threshold to find seizure candidates. The dashed blue line marks the EMD detected seizure onset time which is considered when the number of IMFs per window is greater than the individual electrode threshold on at least seven electrodes in the same 30 s period. Patients highlighted in grey had clinically determined seizure onset zones localized to depth electrodes.

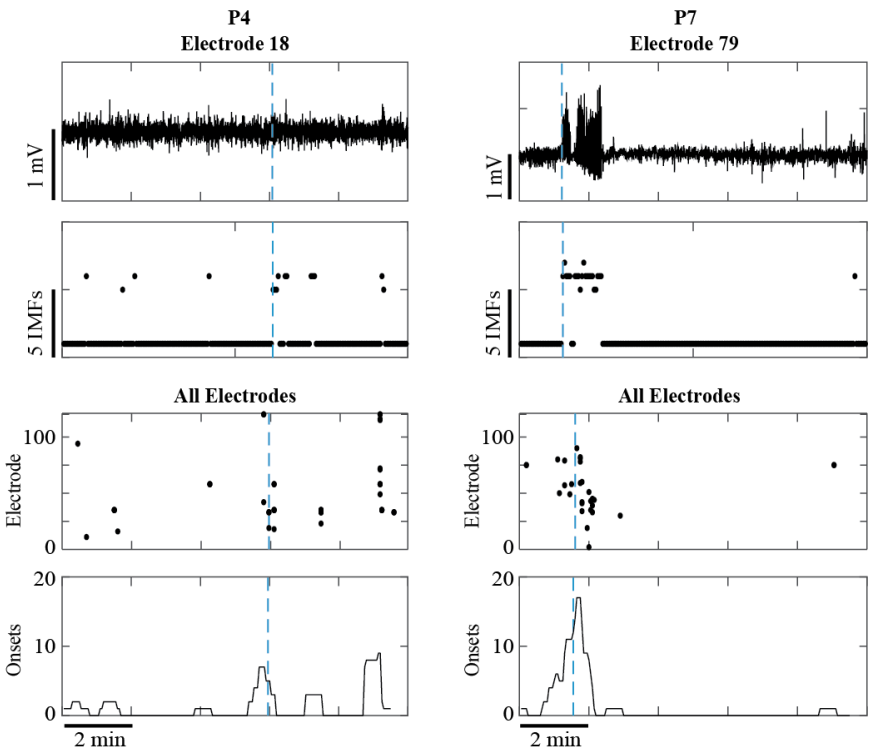

Figure 3.10. False positive detection comparison. Examples of false positives potential seizures detected with the EMD based algorithm and electrographic data from one electrode that crossed the threshold during the potential seizure. The dashed blue line marks the threshold crossing.

IMFs. Signals analyzed in this study showed a change in complexity at seizure onset. The number of IMFs produced by EMD increased at the beginning of a seizure, when compared to non-seizure activity on the same electrode. Since the number of IMFs is a result of the amount of variation in the frequency and amplitude content of the signal, this suggests that there was a significant change in the signal complexity during potential

seizures when compared to non-seizure activity. Similar changes in signal complexity associated with seizure activity have been measured based on signal energy (Bergey & Franaszczuk, 2001).

IMFs have physical meanings in other applications (Norden E Huang, 2005) and features of IMFs, such as mean frequencies and energy content, have been used in seizure detection (Alam & Bhuiyan, 2013). It is possible that, considering the structure that is apparent in the IMFs created by EMD (Figure 3.1), there is some relevant biological meaning in the IMFs that could be useful in seizure detection or studies of epileptogenesis.

Depth electrodes. The EMD based algorithm used here performed notably better on some patient's data than others. This does not appear to be associated with differences in grid location or etiology, but rather the type of electrode to which the seizure onset was localized. Specifically, the algorithm detected 43 of the 45 seizures that were localized to cortical surface electrodes during visual inspection, but only 12 of the 23 seizures on depth electrodes. Tissue, signal and electrode differences could account for the change in detection efficacy observed.

Depth electrodes record activity from deep areas of cortex that is fundamentally different from the activity recorded by surface electrodes (Buzsáki et al., 2012; Zumsteg & Wieser, 2000). Others have noted differences in patterns, duration and frequency of high-frequency oscillations (HFOs) recorded from the cortical surface that were not present in HFOs recorded on depth electrodes (Jirsch et al., 2006). It is possible that there are underlying differences in seizure activity originating from mesial areas when compared to neocortical locations. Such differences may account for the presence or

absence of complexity changes detected with the EMD based algorithm. Some seizures that started on depth electrodes were successfully detected with the EMD based algorithm. This could be an indication of the extent to which the seizure activity spreads or generalizes.

Conclusion. Algorithmic adjuncts to visual inspection could help to objectively identify changes in cortical activity that may be associated with seizures. It is important, however, that these algorithms employ methods that are appropriate for use on biological data. EMD does not assume linearity, stationarity, or signal composition and is data driven. Further investigation and re-parameterization of the EMD based algorithm developed and tested here could improve the sensitivity and specificity of the method, as well as elucidate additional applications for the algorithm, such as studying the propagation of seizure activity. Ultimately, to be accepted into clinical use, any algorithm will need to be extensively tested and validated as well as highly specific, sensitive, and robust.

CHAPTER 4

OBTAINING HIGH QUALITY SIGNALS FROM MICROELECTRODES

Introduction

Electrocorticography (ECoG) was developed in the 1930's as a method to localize seizure activity (Almeida et al., 2005; Penfield, 1939). The design and technique of ECoG has remained essentially unchanged since its introduction and is still a critical part of pre-surgical monitoring for patients with treatment resistant epilepsy. Our understanding of the structure of the cortex, however, has changed since ECoG was introduced.

The neocortex is composed of columnar structures made of highly interconnected, vertically arranged neurons that act as small functional units and have diameters of 300 to 600 μm (Hubel et al., 1977; V. B. Mountcastle, 1997; V. Mountcastle, 1978). Yet, a clinical ECoG electrode records from approximately 20 mm (Menon et al., 1996). The size discrepancy between the scale of cortical computational units and the current clinical recording methods represents an opportunity to improve the specificity of electrophysiological recordings from the cortex. Recognition of this possibility has increased interest in the use of microECoG grids (electrode diameter < 1mm).

Microelectrodes record local field (LFP) and possibly even action potentials (AP) with amplitudes too small to be detected by larger macroelectrodes (diameter >1mm) (Buzsáki et al., 2012; Khodagholy et al., 2014). The precise biophysics and neural circuitry underlying the generation of LFPs is still unknown. Single impulse signals from micro-stimulation transmit through neural tissue by volume conduction so that neural tissue can be modeled as an isotropic resistive medium (Logothetis, Kayser, &

Oeltermann, 2007). However, endogenous LFPs arise from many signal generators and propagate through highly tortuous neural tissue likely by volume conduction, ephaptic, and synaptic mechanisms (Anastassiou et al., 2011; Hales & Pockett, 2014). Regardless of the underlying mechanisms, it is clear that microelectrodes offer improved spatial resolution compared to standard clinical ECoG grids and can detect distinct, functionally and clinically relevant cortical activity (S. S. Kellis et al., 2009; S. Kellis et al., 2010, 2015; Khodagholy et al., 2014; Leuthardt et al., 2009; Pesaran, Pezaris, Sahani, Mitra, & Andersen, 2002; C. a. Schevon et al., 2009; Stead et al., 2010; Wang et al., 2009).

Similar to ECoG grids, microECoG grids are implanted in the subdural space with a pigtail connector routed through the craniotomy, allowing a percutaneous interface to an external amplification and recording system. However, microECoG cannot be treated like ECoG because the change in electrode size has non-trivial implications on the signals recorded and, subsequently, the equipment needed to record them with high fidelity.

Impedance is the amount of resistance generated by a circuit to a current when a voltage is applied to that circuit and varies with frequency. In concert with the electrode diameter, the electrode impedance determines the volume of cortical tissue from which an electrode records signals. Generally, a small electrode, such as a microelectrode, has much higher impedance ($\sim 10^5$ Ω at 1 kHz), records from a smaller volume of tissue and can detect cortical signals of smaller amplitudes than a clinical macroelectrode (impedance $\sim 10^1$ Ω at 1 kHz) which records from a large volume of cortex (~20 mm in any direction) (Menon et al., 1996; C. A. Schevon et al., 2008; Stacey, Kellis, Patel, Greger, & Butson, 2012; Stead et al., 2010).

The particulars of the recording method used become important when recording with microelectrodes where the signals are highly susceptible to noise contamination. ECoG and microECoG recordings use a reference and ground electrode, i.e. pseudo-differential recording. The goal of using a reference is to optimize noise removal at the amplifier using common mode rejection (CMR). To do this, reference electrodes should be lower impedance than and located close to the recording electrode(s) they are coupled with. Further, the wires should travel along the same path through space so they are exposed to the same electromagnetic field noise. The voltage recorded using pseudo-differential recording is the difference between the reference and signal electrode, both of which are tied to a common ground, however, the reference is shared between multiple recording electrodes. Pseudo-differential recording combines the advantages of single-ended and differential recording. Single-ended recording is the simplest method and uses only one electrode. Each signal recorded is tied to a common system ground that is used for CMR at the amplifier. In differential recording, the signal recorded is the voltage difference between a reference and signal electrode that are both tied to the same ground. While differential recording is ideal and is useful where electrical noise is present, it requires twice as many electrodes as single-ended recording and becomes impractical in high channel count recordings.

High impedance electrodes also necessitate changes in the specifications and position of the amplifier. To minimize the amount of 50/60 Hz noise, microphonics and other interferers picked up by the wires, the distance between the recording electrode(s) and the amplifier should be minimized (Harrison, 2008). This is typically accomplished with two amplifiers, the first of which, referred to as the head-stage, is physically small,

positioned as close as possible to the recording site, have a high input impedance, common-mode rejection ratio (CMRR) and dynamic range, low input-referred noise and dc input current, and the ability to block dc offsets. The CMRR refers to how much of the signal common to both the reference (or ground) and signal electrode is removed during CMR. The input-referred noise, which includes all of the voltage and current sources within the amplifier itself that generate noise, should be low enough to capture the smallest amplitudes of an LFP and have a dynamic range large enough to record the full range of an LFP (Harrison, 2008). DC offsets present at the electrode-tissue interface need to be blocked to prevent input voltages that exceed output capabilities (Harrison, 2008; Mohseni & Najafi, 2004). Further, input current multiplies with the electrode-tissue impedance and generates a voltage that causes an error between the real and acquired signal and increases the offset error for the circuit. To minimize this offset, the DC input current from the amplifier should be negligible. Finally, to maximize voltage transfer, the transfer function across the voltage divider created by the electrode and amplifier should be maximized (Stacey et al., 2012). The transfer function is defined by the ratio of the output to input voltage of the voltage divider and is ideally unity (Stacey et al., 2012). In electrophysiology, maximum voltage transfer is achieved by having significantly higher impedance at the amplifier compared to the electrode, thus creating a large voltage drop across the amplifier compared to the voltage drop across the electrode and recorded signals as close as possible to the original signal (Harrison, 2008; Nelson, Pouget, Nilsen, Patten, & Schall, 2008; Stacey et al., 2012). If the electrode impedance is not negligible compared to the amplifier input impedance, frequency-dependent attenuation and phase-shifts may result (Nelson et al., 2008). It is important to note that recording from

microelectrodes with a clinical system can lead to significant waveform distortion, noise introduction and ultimately confused interpretation of signals due to the mismatch of impedances between the electrodes and amplifier (Stacey et al., 2013, 2012).

Ideally, wires exiting the head-stage amplifier should be bundled together, with the ground wire, into a single cable, to ensure that they traverse the same path through space and are exposed to the same noise as they travel to the second-stage amplifier, which performs a second round of CMR and increases the gain of the signals. For electrophysiological recordings, a ground does not refer to earth-ground. Ground refers to a patient-based, low impedance electrode used to record broadband noise from the brain and placed further from the recording electrode(s) than the reference electrode. A patient-based ground electrically isolates the electrodes and the patient from earth ground.

The second stage amplifier should have a high CMRR with which it performs CMR between the output signal of the head-stage amplifier and that recorded on the ground electrode. To record APs and LFPs, the second stage amplifier should have the ability to amplify signals between 10 and 5,000 Hz (Harrison, 2008). Recall the Nyquist Theory to avoid under sampling and aliasing. Nyquist theory states that the highest frequency that can be resolved is half the sampling frequency used to record the data (Nyquist, 2002). The amplifier must also accommodate potentials on the order of hundreds of millivolts. If the amplifier does not have a sufficient voltage range, saturation and loss of information can occur. Lastly, the amount of noise an amplifier adds to the recorded signal, or the noise floor, should be below the amplitude of the electrophysiological signals recorded; hundreds of nano-Volts (Schalk & Leuthardt, 2011).

Shielding can further improve signal quality. Shielding reduces the amount of electromagnetic noise picked up by the wires as they travel through space by insulating each wire individually then wrapping all of the insulated wires together in a conductive layer. Reference and ground electrodes are tied to the conductive layer, effectively creating a signal that contains all system noise that may have been picked up on the recording electrodes. CMR can then remove noise from the recorded signal in a single stage of amplification. Shielding adds considerable bulk to the overall size of the wire bundle and reduces the number of wires and thus, electrodes that can practically be used.

Finally, the recorded signals are digitized. Many systems combine the second-stage amplifier and a digitizer into a single piece of equipment. Once a signal has been digitized, it can be sent significant distances without the risk of noise contamination. The resolution of the analog to digital conversion and the resulting data file size depends on the bit depth of the converter. The bit depth refers to the number of bits used to represent a sample. Electrophysiological signals recorded with microelectrodes attenuate as frequency increases so a bit depth of at least 16-bit should be used to ensure adequate resolution (Schalk & Leuthardt, 2011).

A number of critical aspects need to be considered when designing and recording from microECoG grids. Here, these considerations are presented in a step-by-step description of how to obtain high quality signals from microelectrodes and experiments are performed to show the importance of these aspects.

Protocol

Procedures involving subjects have been approved by the Institutional Review Board at Phoenix Children's Hospital.

Grid design.

Electrode diameter. Choose an electrode diameter. An electrode that records from a volume of tissue similar in scale to that of the cortical process being studied should be considered to avoid volume conduction and spatial averaging of signals. Note that the electrode diameter affects the impedance of the electrode, which in turn affects other system components.

Choose an electrode diameter. An electrode that records from a volume of tissue similar in scale to that of the cortical process being studied should be considered to avoid volume conduction and spatial averaging of signals. Note that the electrode diameter affects the impedance of the electrode, which in turn affects other system components.

Determine desired inter-electrode spacing. Ideally, an electrode grid will capture all of the cortical signals within its recording radius while each electrode within the grid records unique signals. Too large of an inter-electrode spacing can allow important signals to go unrecorded while too small of a space results in oversampling and high correlation between the signals recorded on the electrodes (S. Kellis et al., 2015; Khodagholy et al., 2014; Rubehn, Bosman, Oostenveld, Fries, & Stieglitz, 2009; Stead et al., 2010). Note that the ideal inter-electrode spacing will change with electrode diameter and application.

Position at least one low impedance reference electrode within the same grid and in close proximity to the recording electrodes it is coupled with. Specify wire routing such that reference electrodes are connected to consistent locations on the grid pigtails, which correspond to the reference input on the head-stage (described in 2, below) that will be used. When multiple references are included, assign recording electrodes to each based on spatial proximity.

Consider ground electrode location and wiring. Having a ground electrode within the grid and routing the ground wire through the head-stage and to the second stage amplifier in the same cable as the recording and reference electrodes is preferable as it ensures the wires traverse the same path through space and will be subject to the same noise. A less desirable, but functional method would use an off-grid ground that is brought into either head-stage or second stage amplifier separately.

Head-stage. Design or purchase pigtail connectors that enable head-stage level amplification. The amplifier used in the head-stage should have low input-referred noise (ideally <1μVrms), a large dynamic range (at least +/- tens of mV), negligible DC input current, the ability to block DC offsets (typically around 1-2V), a high CMRR, and an input impedance that is significantly higher than the electrodes (at least 1 GΩ) (Nelson et al., 2008; Stacey et al., 2012). Test each input on the head-stage using a signal generator and the recording system.

Obtain a channel map. Be sure that the layout of the inputs on the head-stage is correct, especially that the reference and ground input locations match the pigtail contact wired to those electrodes.

Equipment positioning. Work with nurses and other care providers to determine a location that will not interfere with the administration of care but will allow access to the equipment when needed. Position large, high voltage equipment away from the patient when possible. The amplifier will need to be close to the patient. Extra care should be taken to secure the amplifier where it is out of the way and cannot fall or be knocked over, will have plenty of slack in the cables connected to the patient and can be accessed safely and easily as needed. Consider the location of outlets and where cords will run as well.

Surgical placement. Obtain informed consent from the patient and/or legal guardians prior to placing microECoG grids. If the patient is a child and over 8 years old, assent should also be obtained.

Identify the desired cortical location to place the microECoG grid. Following the cranial exposure, intraoperative electrocorticography through macroelectrodes can provide insight as to the location of potential sites of interest for monitoring and evaluation with microECoG grid(s).

Position the microECoG grid. Preferably, enough cranial exposure needs to be obtained to allow for direct visualization and then placement of the microECoG grid(s) onto the surface of the brain in the area of interest. Most often, the craniotomy is of sufficient size to directly visualize all of the electrodes. Microelectrodes that are to be placed underneath the intact bone flap are more difficult due to the protrusion of the microelectrodes from the silicon bedding, towards the surface of the brain. In these situations, the electrodes are placed through a combination of strategies including slight

retraction of the brain as well as copious irrigation underneath the grid/microelectrode to "float" the electrodes in place.

Recording. Configure the second stage amplifier. Specify:

- Number of channels that will be recorded
- Sampling frequency. If the equipment used has built in filter levels, be sure that the sampling frequency is high enough that the filters do not occlude meaningful electrophysiological frequencies and that the filters are also set properly.
- Single ended or differential recording
- Referencing mode, i.e. is there one reference that will be shared across all electrodes or are their multiple references that will be used for local channels?
- Grounding mode, i.e. is the connection to the ground electrode coming in through the head-stage or through a separate connection?
- Coupling. AC coupling will block the DC portion of the signal. DC coupling will allow both AC and DC to pass.

Work with a certified technologist (REEGT) to have the head-stages corrected to the microECoG grid pigtails. Plug the opposite end of the cable into the second-stage amplifier. Check all connections to be sure pigtails and plugs are seated properly then turn the second-stage amplifier on.

Begin recording. Assign a code that does not include identifying information under which all data and information collected from the patient with be kept. Visually check the signals being recorded. If possible, extract a short time segment of data and

create a power spectrum to confirm the visual inspection. Check head-stage, second-stage amplifier and ground connections if signals are not acceptable.

Example protocol.

Grid design. A standard 8x8 clinical ECoG grid with macroelectrodes of 3 mm exposed contact diameter, was modified to include 120 microelectrodes, each 75 μm in diameter with approximate impedances of 10^5 Ω at 1 kHz (Figure 4.1) (S. Kellis, Greger, Hanrahan, House, & Brown, 2011).

Reference electrodes were 3 mm in diameter with an impedance of approximately 10^1 Ω at 1 kHz and were added to the sides of the standard 8x8 grid. Microelectrodes were wired to contacts on separate pigtails than the clinical macroelectrodes. Each reference electrode was then wired to the 17^{th} contact position of four microelectrode pigtails. The specific pigtail each reference was wired to was based on that electrode's spatial proximity to the microelectrodes wired to the same tail.

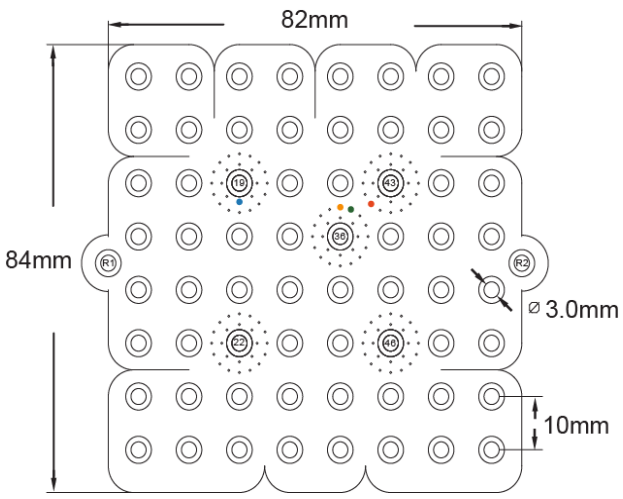

Figure 4.1. Joint macro and microECoG grid. A standard 8x8 clinical ECoG grid was modified to incorporate 120 microelectrodes. Reference 1 (R1) is on the left and reference 2 (R2) is on the right. Electrodes 19, 22, 36, 43 and 46 are surrounded by 24 microelectrodes, each. Microelectrodes around electrodes 19 and 22 and half of those around electrode 36 terminate to a pigtails with R1 as a reference. The remaining microelectrodes use R2 as a reference. The microelectrodes used to generate Figure 4.2 are highlighted. Figure 4.2 A was recorded on the green microelectrode. Figure 4.2 B was the orange microelectrode. Figure 4.2 C was created with the blue microelectrode and Figure 4.2 D is based on the red microelectrode.

Head-stage amplifier. The second-stage amplifier used in this experimental protocol splits the 128 recording channels into banks of 16 and has additional reference and ground pins for each bank. To utilize all recording channels available and minimize the distance between the recording electrodes and the first stage of amplification, head-stage amplifiers were designed using 17 contact GATE-LOK pigtail connectors (PMT

Corporation, Chanhassen, MN USA) and AD8244 unity gain buffer amplifiers (Analog Devices, Norwood, MA USA). The low noise buffers can handle input voltages between 0 to 4 V, have an input impedance of 10 TΩ, negligible DC input current of 2 pA, a dynamic frequency range up to 3 MHz, a maximum offset of 3 μV/^{o}C and a high CMRR indicated by a total system error of only 0.03%. The 17th contact position in the pigtail connectors is for the reference.

Second stage of amplification. A PZ5 NeuroDigitizer (Tucker Davis Technologies, Alachua, FL USA) was used as a second stage amplifier. The amplifier has an input range of +/- 500 mV, input noise of 0.75 μVrms and input impedance of 1 GΩ. PZ5 also contains a digitizer with 28-bit resolution. The second-stage amplifier was configured for DC-coupled recordings using local referencing, an off-grid ('external') ground, 6.1 kHz sampling frequency and the anti-aliasing filter was set to 45% of the sampling frequency.

Grounding. The off-grid, or external ground was a low impedance (~10^{1} Ω at 1 kHz) macroelectrode (3 mm exposed contact diameter) that was placed away from the recording grid during surgery by sliding it beyond the cranial exposure.

Recording. To demonstrate the importance of the components described above, each 16-channel bank of microelectrodes was recorded under different configurations for 10 minutes (Figure 4.2).

Bank A configuration. Microelectrodes and a grid-based reference electrode were connected to a head-stage amplifier. The wires exiting the head-stage were bundled together into a single cable, which was then connected to the second-stage amplifier through a mini-DB26 connector. No ground electrode was used (Figure 4.2 A).

Bank B configuration. Microelectrodes were connected to a head-stage amplifier, but no reference electrode was used. The wires exiting the head-stage were bundled together into a single cable, which was then connected to the second-stage amplifier through a mini-DB26 connector. The second-stage amplifier was set to accept an external ground, which was attached to a stand-alone macroelectrode (3 mm exposed contact diameter) that was slid beyond the cranial exposure during surgery (Figure 4.2 B).

Bank C configuration. Microelectrodes and a grid-based reference electrode were connected to a passive (no CMR performed) pigtail connector. The wires exiting the connector were bundled together into a single cable, which was then connected to the second-stage amplifier through a mini-DB26 connector. No head-stage amplifier was used. The second-stage amplifier was set to accept an external ground, which was attached to a stand-alone macroelectrode (3 mm exposed contact diameter) that was slid beyond the cranial exposure during surgery (Figure 4.2 C).

Bank D configuration. Microelectrodes and a grid-based reference electrode were connected to a head-stage amplifier. The wires exiting the head-stage were bundled together into a single cable, which was then connected to the second-stage amplifier through a mini-DB26 connector. The second-stage amplifier was set to accept an external ground, which was attached to a stand-alone macroelectrode (3 mm exposed contact diameter) that was slid beyond the cranial exposure during surgery (Figure 4.2 D).

Results

This section illustrates the signal quality that can be obtained from subdural microECoG grids implanted in patients with epilepsy, when the above steps are followed. To demonstrate the importance of good recording practices, signals were recorded under

multiple configurations. All analyses were performed using MATLAB (MathWorks Incorporated, Natick, MA, USA). Data were high-pass filtered at 3 Hz using a fifth order Butterworth filter to remove DC offsets. No other filtering or pre-processing was done. Despite proper use of a reference electrode and head-stage level amplification, the absence of a good ground electrode generated significant levels of noise that overshadowed the actual signal recorded (Figure 4.2 A). Removing the head-stage level amplifier had similar effects on signal quality as removing the reference electrode (Figure 4.2 B-C). Signal quality was improved compared to the missing ground configuration, but there is still a clear peak at 60 Hz in the spectrum, indicating noise contamination. Using a reference embedded in the microECoG grid, head-stage level amplification, and a distant patient based ground, a clean signal with little or no noise contamination was recorded (Figure 4.2 D).

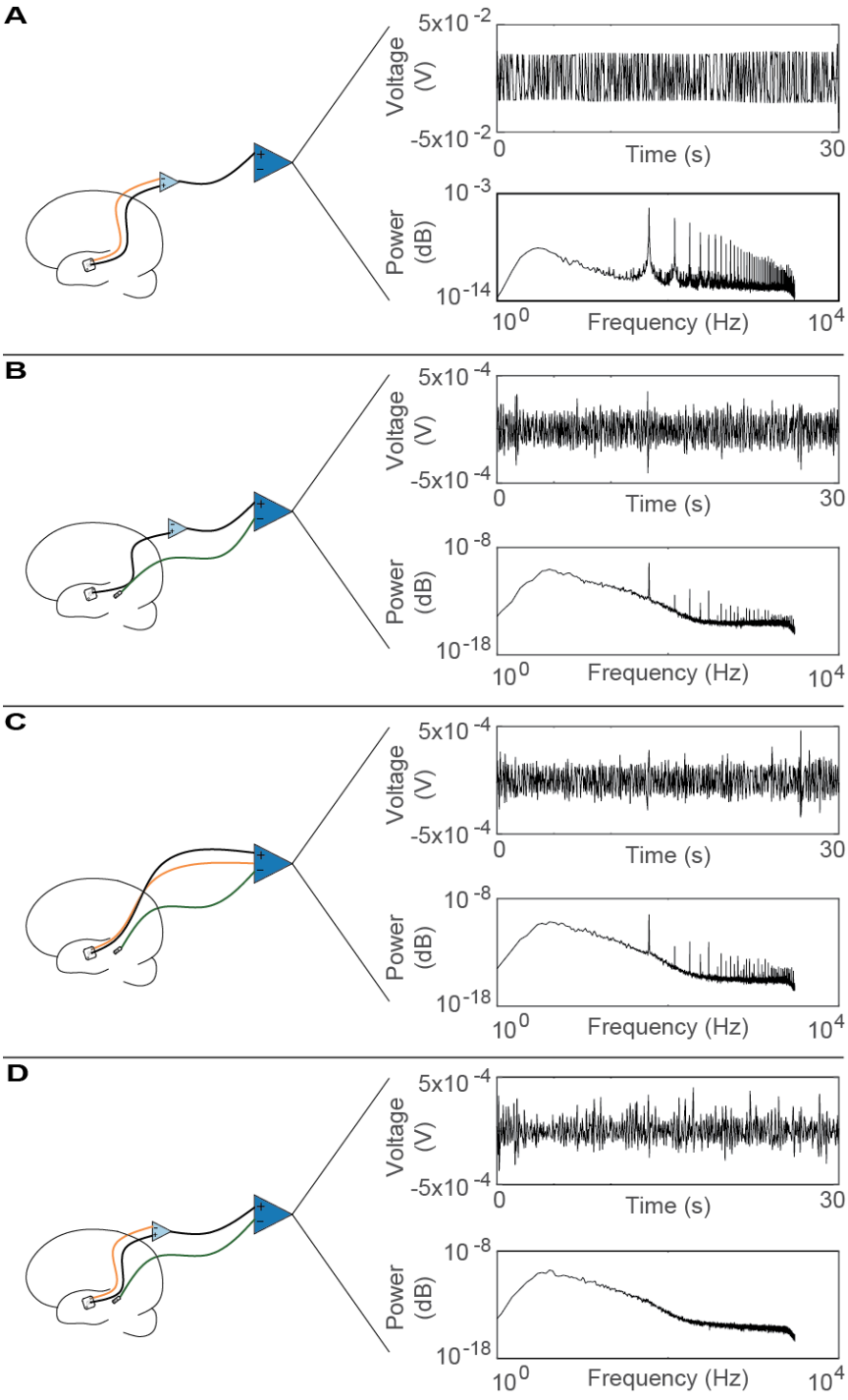
A
5x10 -2
Voltage (V)
-5x10 -2
0
Time (s)
30
10 -3
Power (dB)
10 -14
10 0
Frequency (Hz)
10 4
B
5x10 -4
Voltage (V)
-5x10 -4
0
Time (s)
30
10 -8
Power (dB)
10 -18
10 0
Frequency (Hz)
10 4
C
5x10 -4
Voltage (V)
-5x10 -4
0
Time (s)
30
10 -8
Power (dB)
10 -18
10 0
Frequency (Hz)
10 4
D
5x10 -4
Voltage (V)
-5x10 -4
0
Time (s)
30
10 -8
Power (dB)
10 -18
10 0
Frequency (Hz)
10 4

Figure 4.2. Example recording configurations and resulting signals. The images on the left show the recording configuration used to collect the 30 s data shown on the right. The small, light blue triangle represents the head-stage level amplification. The large, dark blue triangle is the second stage of amplification. The orange line represents the reference electrode wire and the green line is the ground electrode wire. Below each signal is the corresponding log-log spectrum. **(A)** shows the results of not using a ground electrode **(B)** shows signals recorded without a reference electrode **(C)** was recorded without a head-stage and **(D)** had all necessary components to record high quality signals. The signals shown in (B-D) were recorded at the same time. Due to equipment constraints, the data shown in (A) were recorded during a different time epoch.

Discussion

Current techniques used for cortical surface recordings use dated technology. Activity recorded with macroelectrodes is some sort of spatial summation of underlying processes. The large scale over which signals are combined obscures functionally and clinically relevant cortical functions.

To capture the full utility of microelectrodes it is important to record from them properly. Despite their similarities, the difference in impedance of microelectrodes and macroelectrodes necessitates changes in the recording system. High quality signals can be obtained with proper grid design, referencing, grounding and amplification. Shielding may also be useful in low channel count recordings.

Microelectrodes are exciting tools that can record a range of useful signals (S. Kellis et al., 2015; Khodagholy et al., 2014; Leuthardt et al., 2009; Rubehn et al., 2009;

Stead et al., 2010). The increased impedance of microelectrodes, when compared to macroelectrodes, significantly reduces the recording radius and thus the number of ionic processes underlying the LFP signal recorded. The spatial extent of electrophysiology recorded on microelectrodes matches the scale of fundamental computational units of the brain (Stead et al., 2010). Our understanding of the exact components and interactions that generate these signals and how they relate to high-level cortical function and processing continues to grow (S. Kellis et al., 2010; Schalk, 2015; C. A. Schevon et al., 2008). The microelectrode LFP can probe the knowledge gap between single unit recordings and broad activity seen on macroelectrodes and could fuel new scientific inquiries into the underlying mechanisms of cortical function and disorders.

CHAPTER 5

CORTICAL AND ELECTROGRAPHIC SCALES

Introduction

Electrocorticography (ECoG) was developed in the 1930's as a method to localize seizures in patients with treatment resistant epilepsy and is still a prominent part of the evaluation process used today. ECoG electrodes are typically arranged in a grid that is placed in the sub-dural space over the area of the brain thought to house the seizure onset zone. Following the placement surgery, patients will then enter the Epilepsy Monitoring Unit (EMU) for up to two weeks of tests and observation. The current "gold-standard" for the evaluation of a patient's cortical activity is visual inspection of the ECoG data by an epileptologist. In order to proceed with the surgical resection, the clinical team needs to be confident that the patient has focal seizures that do not occur in areas of eloquent cortex (Snead, 2001). That is, that removing the identified area of the brain will not impact critical daily functions such as moving or speaking, and that the patient will be seizure-free after the resection.

A typical ECoG electrode is 4-5 mm in overall diameter, with a recording contact surface of 2-3 mm in diameter. A grid or strip may contain as many as 64 electrodes spaced 10 mm apart, center-to-center. ECoG arrays are placed below the skull, but do not penetrate the cortical surface. Thus their vulnerability to movement artifacts is reduced and spatial resolution is increased compared to EEG, while their estimated duration of functional life and stability is increased compared to penetrating electrodes, which initiate a complicated foreign body response (S. S. Kellis et al., 2009; Schalk & Leuthardt, 2011). Sampling frequencies are typically 250-500 Hz, depending on the institution.

Despite ECoG's widespread and efficacious use, the technique has not kept pace with our growing understanding of cortical form and function. The neocortex is composed of heavily interconnected, vertically arranged columns, that act as the basic unit of operation and are an order of magnitude smaller and range between 300 and 600 μm in diameter (V. B. Mountcastle, 1997; V. Mountcastle, 1978). Functionally and clinically relevant cortical activity has been recorded at spatial scales similar to individual cortical columns (S. S. Kellis et al., 2009; Schmidt et al., 1996; Stead et al., 2010). Yet, a macroelectrode records gross surface field potentials that are composed of some sort of spatial average of simultaneous ionic processes within its recording area; as much as 20 mm in any one direction (Buzsáki et al., 2012; Menon et al., 1996). Thus, a macroelectrode simultaneously records signals from multiple locations containing micro scale activity and in doing so, obscures the individual waveforms or fails to record them altogether.

Microelectrodes (diameter <1mm) arranged in a high-density grid, i.e. microECoG grids, can provide better specificity and sensitivity than clinical ECoG grids, which use macroelectrodes. Similar to ECoG grids, microECoG grids are placed in the sub-dural space but do not penetrate the cortical surface. Unlike ECoG grids, the microelectrodes used in microECoG grids have a high impedance which significantly decreases the amount of cortical volume within the electrodes' recording radius; each microelectrode records from a cortical volume on the sub-millimeter scale and can decipher cortical activity that occurs at amplitudes too small to be detected with macroelectrodes (Schalk & Leuthardt, 2011; C. A. Schevon et al., 2008; Stead et al., 2010). Microelectrodes record signals produced by time evolving activity in small

neuronal populations, individual cortical columns (i.e. local field potentials (LFPs)) or even individual neurons near the microelectrode (i.e. action potentials (APs)) (S. S. Kellis et al., 2009; Khodagholy et al., 2014; Stead et al., 2010). The precise biophysics and neural circuitry that create LFPs is still unknown. Micro-stimulation models suggest that single impulse signals transmit through neural tissue by volume conduction and that neural tissue can subsequently be modeled as an isotropic resistive medium (Logothetis et al., 2007). However, endogenous LFPs arise from many signal generators and propagate through complex neural tissue, likely by a combination of volume conduction, ephaptic, and synaptic mechanisms (Anastassiou et al., 2011; Hales & Pockett, 2014). Regardless of the exact neural mechanisms, compared to clinical macroelectrodes, the specificity of the recordings is improved because there is less spatial averaging and the sensitivity is increased because fewer ionic processes are superimposed to produce the signal recorded.

Clinical diagnosis, knowledge and understanding of epilepsy have been predicated on two extremes for decades; signals collected from individual neurons from animal models of *in vitro* tissue preparations, or massive neuronal populations, as recorded with macroelectrodes. By providing access to local field potentials, microelectrodes could serve as a useful tool to bridge the recording gap between single unit activity and macroelectrode waveforms and provide critical information needed to further our understanding of the biophysical underpinnings of epileptogenesis and cortical function in general. An important step in that process will be developing an understanding of how the signals recorded on microECoG grids relate to those from other, well-established recording modalities. Although studies have simultaneously recorded from macro and microelectrodes, a better understanding of what is recorded by

microelectrodes and how it is physiologically relevant is needed before they will be widely used in the clinical environment.

The present study aimed to investigate the relationship between signals recorded on macro and microelectrodes. To this end, a novel grid was designed that incorporated 120 microelectrodes, each 75 μm in diameter, with a standard 8x8 clinical ECoG grid (64 macroelectrodes, each with an exposed contact diameter of 3 mm). The microelectrodes were arranged in consecutive circles of 8 and 16 electrodes around each of 5 macroelectrodes. It was hypothesized that the signals recorded on the microelectrodes could be combined using a spatially weighted average to generate a signal similar to that of the corresponding macroelectrode.

Materials and Methods

Patients. The Phoenix Children's Hospital Institutional Review Board approved this study and informed consent was received from the patient's parents.

Data from one patient admitted to the pediatric epilepsy monitoring unit (PEMU) at Phoenix Children's Hospital (PCH) (Phoenix, AZ USA) were collected. The placement of sub-dural grids and subsequent monitoring was performed as standard of care for Phase II evaluation of treatment resistant epilepsy to localize the seizure focus and determine suitability for resection surgery. One grid used combined micro and macroelectrodes, which terminated to separate transcutaneous pigtails. The grid was specifically designed to be clinically indiscernible, meaning the macroelectrodes were recorded for the duration of the needed evaluation, without interruption, on the clinical recording system and the microelectrodes were recorded on the research system. When the epileptologists had collected sufficient data, permission was granted to bring one

clinical pigtail into the research recording system such that 16 macroelectrodes (macroelectrodes 33 - 48) were recorded concurrent with 112 microelectrodes.

Grid design. An ECoG grid containing standard clinical macroelectrodes and microelectrodes was designed and manufactured by PMT Corporation (Chanhassen, MN USA) (Figure 5.1).

Data acquisition. When sufficient data to localize seizure onset had been collected, one pigtail associated with clinical macroelectrodes 33 – 48 was brought into the PZ5 NeuroDigitizer and RZ system (Tucker Davis Technologies, Alachua, FL USA). The macroelectrodes and remaining 112 microelectrodes were recorded at 12.2 kHz for approximately 30 minutes. Raw data were visually inspected. A 10 minute segment that was free of high-amplitude activity was isolated and used in the rest of the analysis.

Analysis. All analyses were performed using MATLAB (MathWorks Incorporated, Natick, MA USA). Data were bandpass filtered between 2 and 2000 Hz with a third order Butterworth filter.

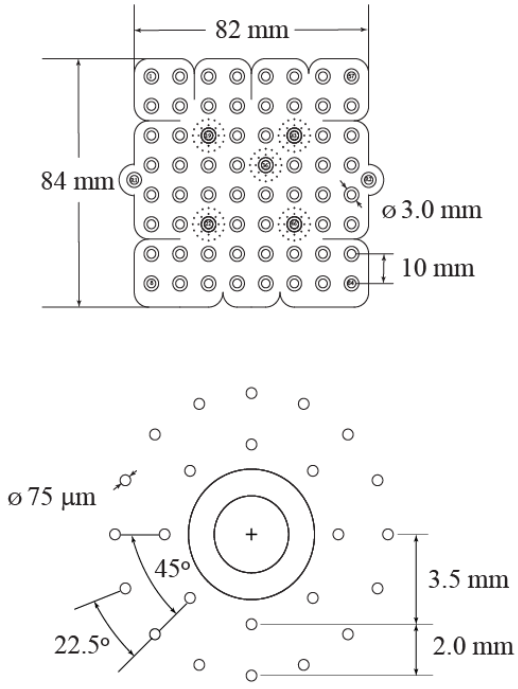

Figure 5.1. Joint macro and micro ECoG grid design. The grid was based on a standard clinical grid with 64 macroelectrodes that were 5.08 mm in overall diameter with an exposed contact diameter of 3 mm and an inter-electrode spacing of 10 mm, center to center, arranged in a standard 8x8 pattern. Surrounding each of five macroelectrodes (19, 22, 36, 43, and 46) were 24 microelectrodes, 75 μm in diameter. The microelectrodes were arranged in two concentric circles. Eight microelectrodes equally spaced at 45 degrees center to center made up the inner circle that was 7 mm in diameter; 2 mm from the outer edge of the contact area of the macroelectrode. The outer circle was 11 mm in diameter and consisted of 16 microelectrodes equally spaced with 22.5 degrees center-to-center separation. Two additional macroelectrodes (R1 and R2), 3 mm in contact diameter, were added on opposing sides of the standard 8x8 grid to serve as reference

electrodes for the microelectrodes. One reference electrode was routed to each of the microelectrode pigtails. Macroelectrodes and microelectrodes terminated to separate pigtails.

Spatially weighted contribution. Following the preprocessing steps outlined above, the signals collected from the microelectrodes surrounding a given macroelectrode were combined into a single signal based on the linear distance from the center of the microelectrode to the center of the macroelectrode. This assignment was performed for each of the 24 microelectrodes surrounding a single macroelectrode. Equation 5.1 summarizes this approach.

$$M_i(t) = \frac{\left[a\left(\frac{\sum m_{j,i}(t)_1}{b}\right)+c\left(\frac{\sum m_{k,i}(t)_2}{d}\right)\right]}{f} \quad (5.1)$$

Here, $M_i(t)$ is the signal recorded from macroelectrode i, with $i = 1,2 \ldots, n$. Where n is the number of macroECoG electrodes surrounded by microelectrodes. $m_{j,i}(t)_1$ is the amplitude, in volts, of the signal recorded on microelectrode j from the first circle surrounding macroECoG electrode i, with $j = 1,2 \ldots, b$, and $m_{k,i}(t)_2$ is the amplitude of the signal, in volts, recorded on microelectrode k from the second circle surrounding macroECoG electrode i, with $k = 1,2 \ldots, d$. a, b, c, d and f are scaling variables. For this study, $n = 3$, $a = 5.5/3.5$, $b = 8$, $c = 1$, $d = 16$ and $f = 2$.

Time domain analysis. Signal similarities were studied by calculating the correlation coefficients for each spatially weighted microelectrode signal and corresponding macroelectrode signal set based on the bandpass filtered data. Next, to monitor the similarities over time, the correlation coefficient was calculated in 1 s windows over the 10 minute data set. The windowed correlation coefficient calculations

were performed to each macro/micro grouping individually, then the three groups were averaged together and the standard error was calculated. A third-degree polynomial was used to calculate a trend line to show changes in the amount of correlation over time.

To visualize raw waveforms, a third order Butterworth notch filter was applied to both the bandpassed macroelectrode and spatially weighted microelectrode signals to remove 55-65 Hz frequencies before plotting.

Frequency domain analysis. The frequency content of the bandpass filtered macroelectrode signal was compared to that of the corresponding spatially weighted microelectrode signal. Power spectral analysis was performed using a ninth order power spectrum and an FFT length of 2^{14}, with 95% confidence intervals. Magnitude-squared coherence estimates were also performed, using an FFT length of 2^{14}, for each signal set. Finally, the average coherence values and the standard error across the three signal sets were calculated.

Results

Data from one patient undergoing monitoring for treatment-resistant epilepsy were collected using a custom ECoG grid that combined macro and microelectrodes.

The spatially weighted contribution method was able to generate signals that matched some portions of the corresponding macroelectrode signals, but did not perform well across the full dataset (Figure 5.2).

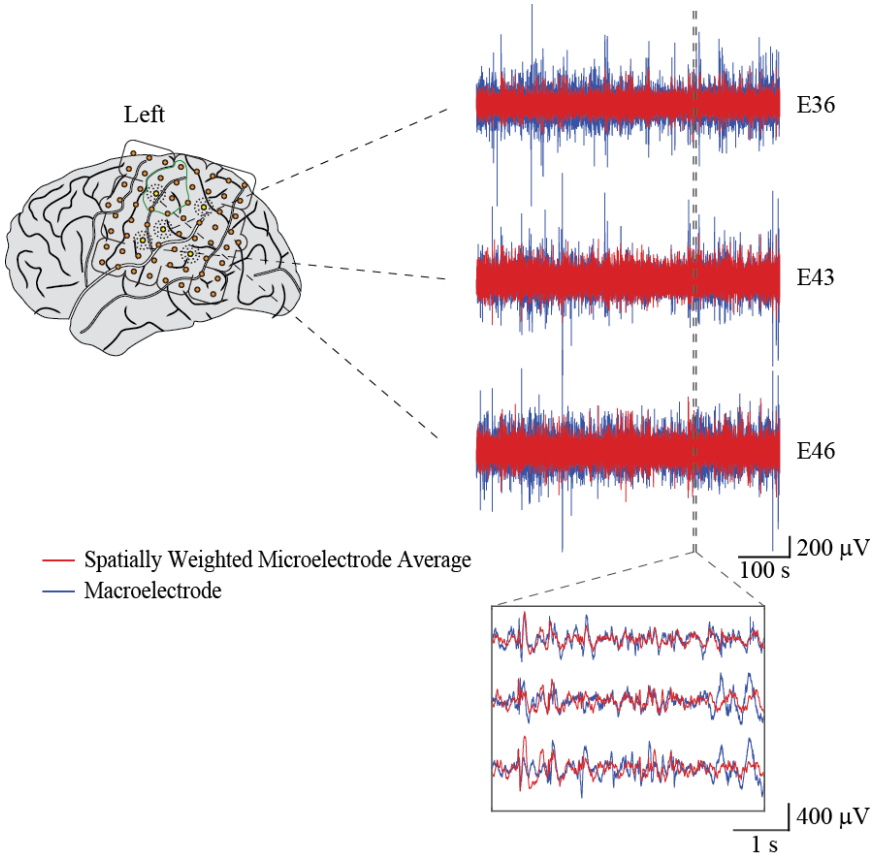

Figure 5.2. Joint macro and microECoG grid placement and resulting signals macroelectrode signals with corresponding spatially weighted microelectrode signals. **(Left)** The grid straddled the central sulcus and a cortical lesion, outlined in green, immediately posterior to the sulcus on the left side of the patient's brain. Macroelectrode 46 and the 24 corresponding microelectrodes, referred to as E46, were positioned directly over the lesion. **(Right)** A 10 minute segment of the spatially weighted microelectrode signal (red) is plotted with the corresponding macroelectrode signal (blue), after bandpass (2 - 2000 Hz) and notch (55 – 65 Hz) filtering. A 5 s sample is displayed to show detail.

The average correlation coefficient across the three signal sets (E36, E43 and E46) was variable across the full 10 minute data segment and did not have prominent trends (Figure 5.3).

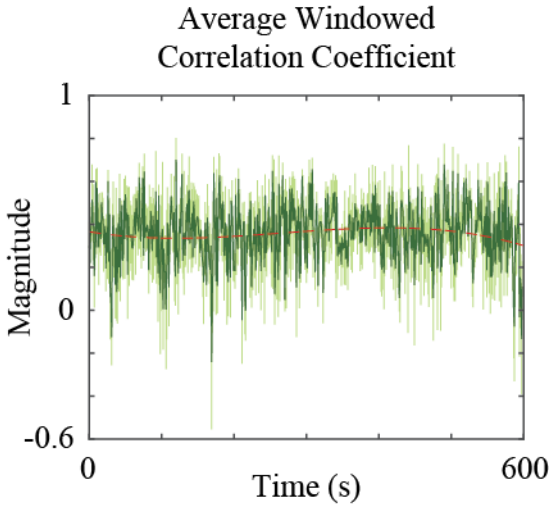

Figure 5.3. Average windowed correlation coefficient. The average correlation coefficient for 1 s of data windowed across time the full 10 min data segment is in dark green and the standard error shown is in light green. A trend line using a third degree polynomial least squares fit is shown with a dashed red line ($p(x) = -0.0006x + 0.3654$).

The spatially weighted microelectrode signal generated by the microelectrodes around macroelectrode 36 correlated with the macroelectrode signal better than the other signal sets while the correlation between macroelectrode 46 and the spatially weighted microelectrode signal was the lowest of the three sets analyzed (r (E36) = 0.5382, r (E43) = 0.2817, r (E46) = 0.2587, $N = 7324247$, $p = 0.05$).

The frequency content within the spatially weighted microelectrode signal and the corresponding macroelectrode signal had a stronger relationship in frequencies below 200 Hz for all signal sets (E36, E43 and E46) (Figure 5.4). The frequency contents of the E36 signal set had the most robust relationship below 200 Hz while E46 was the least related.

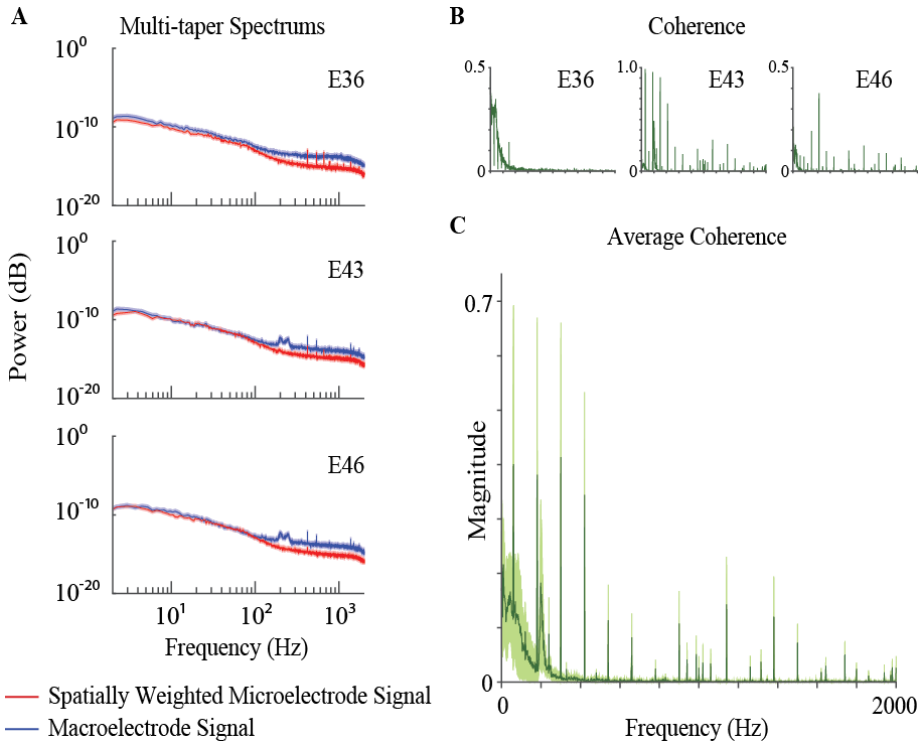

Figure 5.4. Frequency domain comparison between macroelectrodes and the corresponding spatially weighted microelectrode signals. **(A)** The log-log power spectrums of macroelectrodes 36, 43 and 46 shown in blue, with the corresponding spatially weighted microelectrode signal log-log power spectrum shown in red. 95% confidence intervals for the macroelectrode signal and the spatially weight microelectrode signal is shown in light blue and red, respectively. **(B)** The magnitude-

squared coherence estimates for each macro/spatially weighted microelectrode signal set between 2 and 2000 Hz. **(C)** The average magnitude-squared coherence across all three signal sets (E36, E43, E46) within the bandpass filter frequency range (2-2000 Hz) shown in dark green, with the standard error shown in light green.

Discussion

Time domain. Raw signals show that portions of the macroelectrode waveforms are modeled well by the spatially weighted contribution microelectrode signal while other parts are not (Figure 5.2). The differences between the calculated signals and the macroelectrode signals did not appear to be due to a single event or cluster of events, as evidenced by the variable average windowed correlation coefficients across the full 10 minutes data segment and the low coefficients of the trend line generated (Figure 5.3).

Frequency domain. The spatially weighted contribution model was able to somewhat simulate the low-frequency content of the macroelectrode signal (coherence = 0.15 – 0.4). However, frequencies above 200 Hz could not be reproduced. There could be a number of contributing factors to this result. High frequency signals have low amplitudes and the power of these signals recorded by electrodes may be more susceptible to changes such as the spatial integration of additional signal generators. While high frequency activity on microelectrodes is likely a direct result of an increase action potential activity in the neuronal population near that microelectrode, high frequency activity on macroelectrodes is more ambiguous. An increase in the synchrony of activity within a macroelectrode's recording area could produce a substantial increase in power that cannot be replicated by an increase in neuronal activity detected on a

microelectrode (Ray et al., 2008). Furthermore, the macroelectrodes likely record from deeper portions of cortex than the microelectrodes and the relationship between surface and subsurface high gamma (80-170Hz) activity quickly deteriorates with increasing depth (Watanabe et al., 2012). Though the frequency discrepancy observed here was slightly higher than high gamma, it likely follows a similar trend.

Spatial location. The coherence between the signal generated with the spatially weighted contribution method and the signal from macroelectrode 46 was notably worse than the other two signal sets. This could be due to spatial location with respect to the patient's cortical lesion. E46 was positioned over the lesion and seizure focus while the other two groups were over non-focal areas. The seizure focus was localized to mesial aspects of the lesion based on depth electrode recordings evaluated by an epileptologist. It is possible that the added discrepancy found between electrode 46 and the spatially weighted microelectrode signal is due, in some part, to epileptogenic activity originating from mesial structures that cannot be recorded by the microelectrodes due to their high impedance and small recording radius.

Conclusion. The intent of this study was to elucidate relationships between signals recorded on macro and microelectrodes in an ECoG grid. It is likely that full reconstruction of a macroelectrode signal based on the microelectrode signals collected from the cortical surface around it is not possible. The physical recording constraints (i.e. microelectrode recordings could not be collected from the cortical surface directly below by the macroelectrode) were recognized before data collection began. It is conceivable that this did play a role in the low correlation and coherence values calculated, but other factors such as the electrode impedance and therefore the electrode recording radii and

the spatial location of the electrodes with respect to the patient's cortical lesion were likely also contributing factors to the deviation. Thus far, analysis is limited to data collected from one patient. Additional data recorded from similar grids is needed to further investigate these postulations.

CHAPTER 6

SUMMARY AND CONCLUSIONS

Despite ECoG's widespread and efficacious use, the recording and analysis techniques it is used for have not kept pace with our growing understanding of cortical form and function. The work described in this document focuses on applying engineering concepts and design practices to the use of ECoG in the surgical evaluation of patients with treatment resistant epilepsy. Specifically, the use of a computational algorithm to objectively identify seizure onsets recorded on clinical electrodes, equipment and design considerations to acquire high quality signals from microelectrodes, and the relationship between signals recorded on macro and microelectrodes was studied.

Algorithmic adjuncts to visual inspection

Visual inspection of ECoG data has remained the method of choice for clinicians for over 65 years (Almeida et al., 2005; Binder & Haut, 2013; Penfield, 1939). While there is no substitute for the highly trained human in the interpretation of ECoG data, the process is time consuming and subjective. Trends are moving towards improving the specificity and sensitivity of ECoG recordings via increasing the number of electrodes and sampling rate used. It is likely that the use of computational adjuncts could not only help to objectify and speed up the process now, but will become a necessity in the future.

Computational algorithms can quickly and objectively find signal characteristics that cannot be detected with visual inspection. However, it is important that the algorithm used is appropriate for the analysis of biological signals; it should not assume that the signal is linear, stationary or composed of specific functions and should not require prior knowledge of the signal's shape. Empirical mode decomposition (EMD) is a data driven

algorithm that iteratively breaks complex signals into simpler component signals with varying amplitude and frequency relative to time.

The EMD based algorithm developed here identified potential seizures based on changes in the complexity of ECoG signals. The results suggest that a biological data driven algorithm could serve as a useful tool to objectively identify changes in cortical activity associated with seizures. However, detection algorithms may need to be adapted to different electrode types or particular neural structures.

Implications of Microelectrocorticography in Cortical Interfacing

ECoG has been effectively used to study and diagnose neurological pathophysiology for decades (Almeida et al., 2005; Penfield, 1939; Tripathi et al., 2010). Since its introduction, however, our knowledge of the scale at which the brain processes information and technological capabilities to record neural activity have changed (Buzsáki et al., 2012; S. Kellis et al., 2015; V. B. Mountcastle, 1997; V. Mountcastle, 1978). A signal recorded by a clinical ECoG electrode (macroelectrode; diameter > 1 mm) represents some spatial summation of electrophysiological activity from the highly complex neural circuitry occurring within that electrode's recording radius. Studies have shown that using microelectrodes (<1 mm in diameter) can improve the spatial specificity of ECoG recordings and have generated interest in the potential benefits of microECoG in clinical diagnostic and therapy situations (S. S. Kellis et al., 2009; Schalk & Leuthardt, 2011; Stead et al., 2010).

Though both ECoG and microECoG grids are composed of electrodes resting on the surface of the cerebral cortex, altering the diameter of the electrodes creates non-trivial changes in the physics of the electrode-tissue interface that impact multiple aspects

of the recording system. Specifically, microelectrodes have higher impedances than the macroelectrodes currently used in clinical ECoG grids. Using higher impedance electrodes improves spatial specificity of the recordings because the signals are recorded from a smaller volume of cortex, but it also means that the signals are lower in amplitude, and more susceptible to noise contamination than those recorded with macroelectrodes. Critical aspects of the design and recording process were outlined and the experiments performed showed that proper grounding, referencing, and amplification are critical to obtain high quality neural signals from mircoECoG grids.

Microelectrodes record a range of functionally and diagnostically relevant signals (S. Kellis et al., 2015; Khodagholy et al., 2014; Leuthardt et al., 2009; Rubehn et al., 2009; Stead et al., 2010). Our understanding of the exact components and interactions that generate these signals and how they relate to high-level cortical function and processing continues to grow (S. Kellis et al., 2010; Schalk, 2015; C. A. Schevon et al., 2008; Stead et al., 2010). The spatial extent of electrophysiology recorded on microelectrodes matches the scale of a cortical column, the fundamental computational units of the brain, but there is still uncertainty regarding the significance of the micro-morphology observed on microECoG recordings (Stead, et al., 2010). A better understanding of what is recorded by microECoG and how it is physiologically relevant is needed before they will be widely used in the clinical environment.

To probe the relationship between signals recorded on surface macroelectrodes and microelectrodes, a custom grid containing five center-surround electrode sets was designed and used to record from a patient undergoing monitoring for treatment resistant epilepsy. Microelectrode signals were combined using a spatially weight contribution

method to generate a signal that was then compared to the corresponding macroelectrode signal. Time and frequency analysis of the signals show that there may be some relationship between the microelectrode aggregate and the macroelectrode signals, but there was still significant portions of the macroelectrode signal that were unaccounted for. This was particularly true in frequencies above 200 Hz. The findings suggest that the macroelectrode is recording activity not accessible by the microelectrodes, likely either from deep structures or a product of the spatial integration performed by the macroelectrode. Further testing and analysis, possibly involving the simultaneous recording of surface and depth electrodes is needed to fully parse the relationship.

Future Work

EMD based algorithm. There are, without question, many directions the EMD based algorithm could be taken next. Parameters used to apply the algorithm, such as window and step size, as well as those involved with the thresholds used to define an algorithmically identified seizure candidate, will be revisited. Formal parameter optimization, using methods such as machine learning algorithms, should help to improve the specificity and sensitivity of the algorithm. Ideally, a new set of parameters will make the algorithm robust and applicable to all electrode and cortical structure types, but it is possible that further analysis will show that multiple algorithms are needed to optimize detection efficacy in different cortical or sub-cortical areas.

Once parameter optimization is complete, the usefulness of the EMD based algorithm in other aspects of seizure analysis, such as spatiotemporal propagation, can be studied. Epileptologists will be asked to do a thorough review of the data and identify when a seizure starts and to list, in order, the first five electrodes involved with the

seizure activity found. They will also be asked to review any data clips in which false-positive detections were made. This sort of analysis could lead to a better understanding of the EMD based algorithm's potential usefulness as a seizure detection tool and could help study the complexity associated with different types of seizures or cortical structures.

The EMD based algorithm may also prove effective on other electrode types such as EEG and microelectrodes. If the algorithm presents spatially specific results from ECoG grids, it could improve the localization of seizure activity with EEG, which could help guide the placement of ECoG grids. Further, sub-clinical seizures or those suffered by comatose patients that do not manifest physically may also be detectable. Applying the EMD based algorithm to microECoG data could aid in the understanding of the relationship between the micromorphology of waveforms observed by others on microECoG grids and the classical waveforms associated with seizure activity on clinical ECoG grids.

Finally, the physiological relevance of IMFs will be studied. Others have linked IMFs to physical entities, but it is unknown if the same is true regarding cortical dynamics. If the IMF waveforms are meaningful, it could provide insight into the network dynamics of cortical function and epileptogenesis.

Cortical and electrographic scales. The relationship between signals recorded on electrodes is not only important to show the implications of new types of electrodes in cortical interfacing, but could also provide significant insight about the scales and network dynamics of cortical processing and the spread of pathological conditions. Thus

far, data from one patient has been collected using the specialized grid design. To investigate the initial findings further, additional grids will used to record from patients.

Additionally, based on the results obtained here, a logical and relatively straightforward next step is to simultaneously record depth electrodes with microECoG and macroECoG grids at a high sampling rate (6-12 kHz) from multiple patients to obtain a more complete data set that accounts for activity from multiple depths. This sort of recording could also give insight into the types of signals recorded with depth electrodes and even why the EMD based algorithm developed here did not perform well on signals recorded with them. A more advanced approach that may prove useful would incorporate depth electrodes that have multiple recording sights along the shank to probe a variety of cortical depths and possibly even a shallow penetrating array such as the Utah array to account for more superficial cortical layers. Obviously, the number of recording channels rises quickly in this sort of recording scheme so equipment and electrode design will be a critical aspect of the approach.

Conclusion

The amalgamation of engineering and medicine holds exciting potential and great challenges. It is important that engineers recognize the level of complexity of the human body and brain and work to develop devices and methods appropriately. Ultimately, when done correctly, applying engineering insights and innovation in the clinical realm could bring about novel ways to improve patient care.

The work described here focuses on two potential improvements to the Phase II evaluation process for focal resection surgery; using a computational algorithm to objectify the visual review process and recording from microECoG grids to improve

spatial resolution. While some feasible benefits have been highlighted throughout this document, there is the potential of broader impacts on the field of epilepsy and clinical decision making that can be realized through these sorts of approaches.

Objectivity. The success of focal resection surgery relies on our ability to accurately identify not only the location of a seizure focus, but also the extent of epileptogenic tissue. The identification process, however, is highly subjective and relies heavily on the visual inspection of cortical activity in both Phase I and Phase II evaluations. Using computational analysis methods could help to objectify the process.

Phase I involves measures such as scalp electroencephalography (EEG) recordings and imaging. If there is not a clear indication of cortical malformation in the imaging data, the decision of what type (grid, strip or depth) of sub-cranial electrodes to use and where to place them is determined by the visual inspection of EEG recordings alone. Poor focus identification with EEG can result in incomplete or lack of coverage of the seizure focus with ECoG grids. Incomplete focus coverage creates a situation referred to as edge effect, which is challenging because the full extent of epileptogenic tissue cannot be deduced. The presence of an edge effect could then impact the extent of resection performed and create the potential for lack of seizure freedom following resection. Developing computational analysis methods could help to objectively determine where and when seizures start. Ideally, when applied to EEG data, such methods will enable clinicians to make better informed and objective decisions regarding the type and placement of sub-cranial electrodes, which will ultimately improve localization capabilities with ECoG. Perhaps further work would create three-

dimensional localization capabilities with EEG data that could obviate the need for sub-cranial electrodes in some patients.

Further, if microECoG grids begin to be used in clinical evaluation, accurate localization will be particularly important. MicroECoG can improve the spatial resolution of recordings. This improved spatial resolution could be especially useful in cases of small foci, foci in close proximity to eloquent cortex or disconnection surgeries, where delineation between healthy and epileptogenic tissue is critical. However, within current channel count restrictions and recording capabilities, the smaller electrode size used in microECoG grids creates a trade-off between spatial resolution and coverage. Thus, to maximize the utility of microECoG grids, we must be able to identify, with high, objective certainty, where they need to be placed based on Phase I analysis methods.

Databases. One of the biggest challenges in the treatment of epilepsy is the idiosyncratic nature of the disorders that give rise to seizures. While analysis methods may be useful in seizure detection for individuals, a broader impact on the field is likely to be realized through the concurrent analysis of data from many patients, i.e. a "big data" approach. The analysis of data from many patients will help to highlight trends and commonalities that may not be obvious in small patient populations. This sort of approach could aide in our understanding of the efficacy of monitoring methods, probability of success of particular treatment modalities, and less frequency scenarios such as SUDEP, as well as the identification of acute and disease progression related biomarkers. If incorporated with other biological metrics and outcomes, relationships and indicators may also be found that are not based on cortical activity alone, but instead on a system, or whole patient level. Considering the amount of data this will involve,

computational algorithms will be critical for developing quantitative metrics that can be easily compared and span multiple data formats and collection platforms.

Beyond epilepsy. To this point, methods for improving the evaluation of epilepsy has been discussed, but the computational and signal processing techniques used to study epilepsy could also be applied to other fields. The EEG correlates of Autism, depression, Alzheimer's diseases and many other disorders are being investigated and could benefit from objective, quantitative analysis methods. Further, both microECoG and computational approaches could be useful in studying phenomena such as cortical spreading depression (CSD) that may be associated with cortical insults such as traumatic brain injury, stroke and migraines.

WORKS CITED

Abad, R. S.-C., Sanmartí Vilaplana, F. X., & Serratosa, J. M. (2007). Genetic Causes of Epilepsy. *The Neurologist*, *13*(Supplement 1), S47–S51.

Alam, S. M. S., & Bhuiyan, M. I. H. (2013). Detection of seizure and epilepsy using higher order statistics in the EMD domain. *IEEE Journal of Biomedical and Health Informatics*, *17*(2), 312–8.

Almeida, A. N., Martinez, V., & Feindel, W. (2005). The first case of invasive EEG monitoring for the surgical treatment of epilepsy: Historical significance and context. *Epilepsia*, *46*(7), 1082–1085.

Anastassiou, C. a, Perin, R., Markram, H., & Koch, C. (2011). Ephaptic coupling of cortical neurons. *Nature Neuroscience*, *14*(2), 217–223.

Aschenbrenner-Scheibe, R., Maiwald, T., Winterhalder, M., Voss, H. U., Timmer, J., & Schulze-Bonhage, A. (2003). How well can epileptic seizures be predicted? An evaluation of a nonlinear method. *Brain*, *126*(12), 2616–2626.

Berg, A. T., Berkovic, S. F., Brodie, M. J., Buchhalter, J., Cross, J. H., Van Emde Boas, W., … Scheffer, I. E. (2010). Revised terminology and concepts for organization of seizures and epilepsies: Report of the ILAE Commission on Classification and Terminology, 2005-2009. *Epilepsia*, *51*(4), 676–685.

Bergen, D. C. (2006). Results of Epilepsy Surgery: Still So Much to Learn. *Epilepsy Currents*, *6*(3), 80–82.

Bergey, G. K., & Franaszczuk, P. J. (2001). Epileptic seizures are characterized by changing signal complexity. *Clinical Neurophysiology*, *112*(2), 241–249.

Binder, D. K., & Haut, S. R. (2013). Toward new paradigms of seizure detection. *Epilepsy & Behavior : E&B*, *26*(3), 247–52.

Bizopoulos, P. A., Tsalikakis, D. G., Tzallas, A. T., Koutsouris, D. D., & Fotiadis, D. I. (2013). EEG epileptic seizure detection using k-means clustering and marginal spectrum based on ensemble empirical mode decomposition. In *13th IEEE International Conference on BioInformatics and BioEngineering, IEEE BIBE 2013* (pp. 13–16).

Bulacio, J. C., Jehi, L., Wong, C., Gonzalez-Martinez, J., Kotagal, P., Nair, D., … Bingaman, W. (2012). Long-term seizure outcome after resective surgery in patients evaluated with intracranial electrodes. *Epilepsia*, *53*(10), 1722–30.

Buzsáki, G., Anastassiou, C. a., & Koch, C. (2012). The origin of extracellular fields and currents — EEG, ECoG, LFP and spikes. *Nature Reviews Neuroscience*, *13*(6), 407–420.

Cross, J. H., Jayakar, P., Nordli, D., Delalande, O., Duchowny, M., Wieser, H. G., … Mathern, G. W. (2006). Proposed criteria for referral and evaluation of children for epilepsy surgery: recommendations of the Subcommission for Pediatric Epilepsy Surgery. *Epilepsia*, *47*(6), 952–9.

Dobesberger, J., Ristić, A. J., Walser, G., Kuchukhidze, G., Unterberger, I., Höfler, J., … Trinka, E. (2015). Duration of focal complex, secondarily generalized tonic–clonic, and primarily generalized tonic–clonic seizures — A video-EEG analysis. *Epilepsy & Behavior*, (September).

Douglas, R. J., & Martin, K. a. C. (2004). Neuronal Circuits of the Neocortex. *Annual Review of Neuroscience*, *27*(1), 419–451.

England, M. J., Liverman, C. T., Schultz, A. M., & Strawbridge, L. M. (2012). Epilepsy across the spectrum: Promoting health and understanding. A summary of the Institute of Medicine report. *Epilepsy and Behavior*, *25*(2), 266–276.

F.T., S., M.J., M., & R.E., W. J. (2008). Responsive Cortical Stimulation for the Treatment of Epilepsy. *Neurotherapeutics*, *5*(1), 68–74.

Fathima, T., Bedeeuzzaman, M., Farooq, O., & Khan, Y. U. (2011). Wavelet Based Features for Epileptic Seizure Detection. *MES Journal of Technology and Management*.

Ferree, T. C., Clay, M. T., & Tucker, D. M. (2001). The spatial resolution of scalp EEG. *Neurocomputing*, *38-40*, 1209–1216.

Fisher, R. S., Van Emde Boas, W., Blume, W., Elger, C., Genton, P., Lee, P., & Engel, J. (2005). Epileptic seizures and epilepsy: Definitions proposed by the International League Against Epilepsy (ILAE) and the International Bureau for Epilepsy (IBE). *Epilepsia*, *46*(4), 470–472.

Fourier, J. (1822). *Théorie Analytique de la Chaleur*. Paris: Chez Firmin Didot, père et fils.

Galbarriatu, L., Pomposo, I., Aurrecoechea, J., Marinas, a., Agúndez, M., Gómez, J. C., … Garamendi, I. (2015). Vagus nerve stimulation therapy for treatment-resistant epilepsy: A 15-year experience at a single institution. *Clinical Neurology and Neurosurgery*, *137*, 89–93.

Gerber, P. a, Chapman, K. E., Chung, S. S., Drees, C., Maganti, R. K., Ng, Y.-T., … Kerrigan, J. F. (2008). Interobserver agreement in the interpretation of EEG patterns in critically ill adults. *Journal of Clinical Neurophysiology : Official Publication of the American Electroencephalographic Society*, *25*(5), 241–249.

Geschwind, N., & Kaplan, E. (1962). A human cerebral deconnection syndrome. *Neurology*, 675–685.

Gotman, J. (1983). Measurement of small time differences between EEG channels: Method and application to epileptic seizure propagation. *Electroencephalography and Clinical Neurophysiology*.

Gutiérrez, J., Alcántara, R., & Medina, V. (2001). Analysis and localization of epileptic events using wavelet packets. *Medical Engineering & Physics*, *23*(9), 623–31.

Haar, A. (1911). Zur Theorie der orthogonalen Funktionensysteme. *Mathematische Annalen*, *71*(1), 38–53.

Haas, S. M., Frei, M. G., & Osorio, I. (2007). Strategies for adapting automated seizure detection algorithms. *Medical Engineering & Physics*, *29*(8), 895–909.

Hales, C. G., & Pockett, S. (2014). The relationship between local field potentials (LFPs) and the electromagnetic fields that give rise to them. *Frontiers in Systems Neuroscience*, *8*(December), 1–4.

Halpern, C. H., Samadani, U., Litt, B., Jaggi, J. L., & Baltuch, G. H. (2008). Deep brain stimulation for epilepsy. *Neurotherapeutics*, *5*(1), 59–67.

Harrison, R. R. (2008). The Design of Integrated Circuits to Observe Brain Activity. *Procedings of the IEEE*, *96*(7), 1203–1216.

Hill, N. J., Gupta, D., Brunner, P., Gunduz, A., Adamo, M. A., Ritaccio, A., & Schalk, G. (2012). Recording Human Electrocorticographic (ECoG) Signals for Neuroscientific Research and Real-time Functional Cortical Mapping. *Journal of Visualized Experiments*, (64), 1–5.

Houfek, E. E. M. D., & Ellingson, R. J. P. D. (1959). On the Reliability of Clinical EEG Interpretation. *Journal of Nervouse & Mental Disease*, *128*(5), 425–437.

Howard, P., Twycross, R., Shuster, J., Mihalyo, M., Rémi, J., & Wilcock, A. (2011). Anti-epileptic Drugs. *Journal of Pain and Symptom Management*, *42*(5), 788–804.

Huang, N. E. (2005). INTRODUCTION TO THE HILBERT–HUANG TRANSFORM AND ITS RELATED MATHEMATICAL PROBLEMS (pp. 1–26).

Huang, N. E., Shen, Z., Long, S. R., Wu, M. C., Shih, H. H., Zheng, Q., … Liu, H. H. (1998). The empirical mode decomposition and the Hilbert spectrum for nonlinear and non-stationary time series analysis. *Proceedings of the Royal Society A: Mathematical, Physical and Engineering Sciences*, *454*(1971), 903–995.

Hubel, D. H., Wiesel, T. N., & Stryker, M. P. (1977). Orientation columns in macaque monkey visual cortex demonstrated by the 2-deoxyglucose autoradiographic technique. *Nature*, *269*(5626), 328–330.

Iasemidis, L. D. (2003). Epileptic seizure prediction and control. *IEEE Transactions on Bio-Medical Engineering*, *50*(5), 549–558.

Jirsch, J. D., Urrestarazu, E., LeVan, P., Olivier, a, Dubeau, F., & Gotman, J. (2006). High-frequency oscillations during human focal seizures. *Brain : A Journal of Neurology*, *129*(Pt 6), 1593–608.

Kajikawa, Y., & Schoeder, E. (2012). How local is the local field potential? *Neuron*, *72*(5), 847–858.

Kellis, S., Greger, B., Hanrahan, S., House, P., & Brown, R. (2011). Sensing millimeter-scale dynamics in cortical surface potentials for neural prosthetics. In *Proceedings of IEEE Sensors* (pp. 1823–1826).

Kellis, S., Miller, K., Thomson, K., Brown, R., House, P., & Greger, B. (2010). Decoding spoken words using local field potentials recorded from the cortical surface. *Journal of Neural Engineering*, *7*(5), 056007.

Kellis, S. S., House, P. A., Thomson, K. E., Brown, R., & Greger, B. (2009). Human neocortical electrical activity recorded on nonpenetrating microwire arrays: applicability for neuroprostheses. *Neurosurgical Focus*, *27*(1), E9.

Kellis, S., Sorensen, L., Darvas, F., Sayres, C., O'Neill, K., Brown, R., … Greger, B. (2015). Multi-scale analysis of neural activity in humans: implications for micro-scale electrocorticography. *Clinical Neurophysiology*, 1–11.

Khodagholy, D., Gelinas, J. N., Thesen, T., Doyle, W., Devinsky, O., Malliaras, G. G., & Buzsáki, G. (2014). NeuroGrid: recording action potentials from the surface of the brain. *Nature Neuroscience*, *18*(2), 310–315.

Kossoff, E. H., McGrogan, J. R., Bluml, R. M., Pillas, D. J., Rubenstein, J. E., & Vining, E. P. (2006). A modified Atkins diet is effective for the treatment of intractable pediatric epilepsy. *Epilepsia*, *47*(2), 421–424.

Kwan, P., Arzimanoglou, A., Berg, A. T., Brodie, M. J., Allen Hauser, W., Mathern, G., … French, J. (2010). Definition of drug resistant epilepsy: consensus proposal by the ad hoc Task Force of the ILAE Commission on Therapeutic Strategies. *Epilepsia*, *51*(6), 1069–77.

Kwan, P., & Brodie, M. J. (2000). Early identification of refractory epilepsy. *The New England Journal of Medicine*, *342*(5), 314–9.

Kwan, P., Schachter, S. C., & Brodie, M. J. (2011). Drug-resistant epilepsy. *The New England Journal of Medicine*, *365*(10), 919–26.

Lefevre, F., & Aronson, N. (2000). Ketogenic Diet for the Treatment of Refractory Epilepsy in Children: A Systematic Review of Efficacy. *PEDIATRICS*, *105*(4), e46–e46.

Lehmkuhle, M. J., Thomson, K. E., Scheerlinck, P., Pouliot, W., Greger, B., & Dudek, F. E. (2009). A Simple Quantitative Method for Analyzing Electrographic Status Epilepticus in Rats. *Journal of Neurophysiology*, *101*(3), 1660–1670.

Lehnertz, K. (2008). Epilepsy and nonlinear dynamics. *Journal of Biological Physics*, *34*(3-4 SPEC. ISS.), 253–266.

Leuthardt, E. C., Freudenberg, Z., Bundy, D., & Roland, J. (2009). Microscale recording from human motor cortex: implications for minimally invasive electrocorticographic brain-computer interfaces. *Neurosurgical FOCUS*, *27*(1), E10.

Li, S., Zhou, W., Yuan, Q., Geng, S., & Cai, D. (2013). Feature extraction and recognition of ictal EEG using EMD and SVM. *Computers in Biology and Medicine*, *43*(7), 807–16.

Lodder, S. S., & van Putten, M. J. a M. (2013). Quantification of the adult EEG background pattern. *Clinical Neurophysiology : Official Journal of the International Federation of Clinical Neurophysiology*, *124*(2), 228–37.

Logothetis, N. K., Kayser, C., & Oeltermann, A. (2007). In Vivo Measurement of Cortical Impedance Spectrum in Monkeys: Implications for Signal Propagation. *Neuron*, *55*(5), 809–823.

Ludwig, K. a, Miriani, R. M., Langhals, N. B., Joseph, M. D., Anderson, D. J., & Kipke, D. R. (2009). Using a common average reference to improve cortical neuron recordings from microelectrode arrays. *Journal of Neurophysiology*, *101*(3), 1679–1689.

Menon, V., Freeman, W. J., Cutillo, B. A., Desmond, J. E., Ward, M. F., Bressler, S. L., … Gevins, A. S. (1996). Spatio-temporal correlations in human gamma band electrocorticograms. *Electroencephalography and Clinical Neurophysiology*, *98*(2), 89–102.

Miller, K. D., Pinto, D. J., & Simons, D. J. (2001). Processing in layer 4 of the neocortical circuit: New insights from visual and somatosensory cortex. *Current Opinion in Neurobiology*, *11*(4), 488–497.

Mohseni, P., & Najafi, K. (2004). A Fully Integrated Neural Recording Amplifier with DC Input Stabilization. *IEEE Transactions on Biomedical Engineering*, *51*(5), 832–837.

Mormann, F., Andrzejak, R. G., Elger, C. E., & Lehnertz, K. (2007). Seizure prediction: The long and winding road. *Brain*, *130*(2), 314–333.

Mountcastle, V. (1978). An organizing principle for cerebral function: the unit model and the distributed system. In *The Mindful Brain*.

Mountcastle, V. B. (1997). The columnar organization of the neocortex. *Brain : A Journal of Neurology*, *120 (Pt 4*, 701–22.

Muzykewicz, D. a., Lyczkowski, D. a., Memon, N., Conant, K. D., Pfeifer, H. H., & Thiele, E. a. (2009). Efficacy, safety, and tolerability of the low glycemic index treatment in pediatric epilepsy. *Epilepsia*, *50*(5), 1118–1126.

Nelson, M. J., Pouget, P., Nilsen, E. A., Patten, C. D., & Schall, J. D. (2008). Review of signal distortion through metal microelectrode recording circuits and filters. *Journal of Neuroscience Methods*, *169*(1), 141–157.

Nyquist, H. (2002). Certain topics in telegraph transmission theory. *Proceedings of the IEEE*, *90*(2), 280–305.

O'Brien, D. (1998). Toxic and metabolic causes of seizures. *Clinical Techniques in Small Animal Practice*.

Orosco, L., Laciar, E., Correa, A. G., Torres, A., & Graffigna, J. P. (2009). An epileptic seizures detection algorithm based on the empirical mode decomposition of EEG. *Conference Proceedings : ... Annual International Conference of the IEEE Engineering in Medicine and Biology Society. IEEE Engineering in Medicine and Biology Society. Conference*, *2009*, 2651–4.

Osorio, I., Frei, M. G., & Wilkinson, S. B. (1998). Real-time automated detection and quantitative analysis of seizures and short-term prediction of clinical onset. *Epilepsia*, *39*(6), 615–27.

Oweis, R. J., & Abdulhay, E. W. (2011). Seizure classification in EEG signals utilizing Hilbert-Huang transform. *Biomedical Engineering Online*, *10*(1), 38.

Pachori, R. B., & Bajaj, V. (2011). Analysis of normal and epileptic seizure EEG signals using empirical mode decomposition. *Computer Methods and Programs in Biomedicine*, *104*(3), 373–81.

Pardalos, P. M., Wanpracha Chaovalitwongse, Iasemidis, L. D., Chris Sackellares, J., Shiau, D.-S., Carney, P. R., … Yatsenko, V. a. (2004). Seizure warning algorithm based on optimization and nonlinear dynamics. *Mathematical Programming*, *101*, 365–385.

Penfield, W. (1939). The Epilepsies: With a Note on Radical Therapy. *New England Journal of Medicine*.

Penry, K. (1981). Proposal for revised clinical and electroencephalographic classification of epileptic seizures. From the Commission on Classification and Terminology of the International League Against Epilepsy. *Epilepsia*, *22*(4), 489–501.

Pesaran, B., Pezaris, J. S., Sahani, M., Mitra, P. P., & Andersen, R. a. (2002). Temporal structure in neuronal activity during working memory in macaque parietal cortex. *Nature Neuroscience*, *5*, 805–811.

Ray, S., Crone, N. E., Niebur, E., Franaszczuk, P. J., & Hsiao, S. S. (2008). Neural Correlates of High-Gamma Oscillations (60-200 Hz) in Macaque Local Field Potentials and Their Potential Implications in Electrocorticography. *Journal of Neuroscience*, *28*(45), 11526–11536.

Rosso, O. a., Blanco, S., & Rabinowicz, A. (2003). Wavelet analysis of generalized tonic-clonic epileptic seizures. *Signal Processing*, *83*(6), 1275–1289.

Rubehn, B., Bosman, C., Oostenveld, R., Fries, P., & Stieglitz, T. (2009). A MEMS-based flexible multichannel ECoG-electrode array. *Journal of Neural Engineering*, *6*(3), 036003.

Samar, V. J., Bopardikar, a, Rao, R., & Swartz, K. (1999). Wavelet analysis of neuroelectric waveforms: a conceptual tutorial. *Brain and Language*, *66*(1), 7–60.

Schalk, G. (2015). A general framework for dynamic cortical function: the function-through-biased-oscillations (FBO) hypothesis. *Frontiers in Human Neuroscience*, *9*(June), 1–10.

Schalk, G., & Leuthardt, E. C. (2011). Brain-computer interfaces using electrocorticographic signals. *IEEE Reviews in Biomedical Engineering*, *4*, 140–154.

Schendel, A. A., Thongpang, S., Brodnick, S. K., Richner, T. J., Lindevig, B. D. B., Krugner-Higby, L., & Williams, J. C. (2013). A cranial window imaging method for monitoring vascular growth around chronically implanted micro-ECoG devices. *Journal of Neuroscience Methods*, *218*(1), 121–130.

Schevon, C. A., Ng, S. K., Cappell, J., Goodman, R. R., McKhann, G., Waziri, A., … Emerson, R. G. (2008). Microphysiology of epileptiform activity in human neocortex. *Journal of Clinical Neurophysiology : Official Publication of the American Electroencephalographic Society*, *25*(6), 321–330.

Schevon, C. a., Trevelyan, a. J., Schroeder, C. E., Goodman, R. R., McKhann, G., & Emerson, R. G. (2009). Spatial characterization of interictal high frequency oscillations in epileptic neocortex. *Brain*, *132*(11), 3047–3059.

Schiff, S. J. (1994). Fast wavelet transformation of EEG. *Electroencephalography and Clinical Neurophysiology*, *91*, 442–455.

Schindler, K., Leung, H., Elger, C. E., & Lehnertz, K. (2007). Assessing seizure dynamics by analysing the correlation structure of multichannel intracranial EEG. *Brain*, *130*(1), 65–77.

Schmidt, E. M., Bak, M. J., Hambrecht, F. T., Kufta, C. V, O'Rourke, D. K., & Vallabhanath, P. (1996). Feasibility of a visual prosthesis for the blind based on intracortical microstimulation of the visual cortex. *Brain : A Journal of Neurology*, *119 (Pt 2*, 507–522.

Shimizu, H., & Maehara, T. (2000). Neuronal disconnection for the surgical treatment of pediatric epilepsy. *Epilepsia*, *41 Suppl 9*, 28–30.

Shinnar, S., Berg, A. T., Moshe, S. L., & Shinnar, R. (2001). How long do new-onset seizures in children last? *Annals of Neurology*, *49*(5), 659–664.

Snead, O. C. I. (2001). Surgical Treatment of Medically Refractory epilepsy in Childhood. *Brain and Development*, *23*, 199–207.

Stacey, W. C., Kellis, S., Greger, B., Butson, C. R., Patel, P. R., Assaf, T., … Glynn, S. (2013). Potential for unreliable interpretation of EEG recorded with microelectrodes. *Epilepsia*, *54*(8), 1391–1401.

Stacey, W. C., Kellis, S., Patel, P. R., Greger, B., & Butson, C. R. (2012). Signal distortion from microelectrodes in clinical EEG acquisition systems. *Journal of Neural Engineering*.

Staley, K., Hellier, J. L., & Dudek, F. E. (2005). Do interictal spikes drive epileptogenesis? *The Neuroscientist : A Review Journal Bringing Neurobiology, Neurology and Psychiatry*, *11*(4), 272–276.

Stead, M., Bower, M., Brinkmann, B. H., Lee, K., Marsh, W. R., Meyer, F. B., … Worrell, G. a. (2010). Microseizures and the spatiotemporal scales of human partial epilepsy. *Brain : A Journal of Neurology*, *133*(9), 2789–97.

Thomson, A. M., & Lamy, C. (2007). Functional maps of neocortical local circuitry. *Frontiers in Neuroscience*, *1*(1), 19–42.

Tripathi, M., Garg, a., Gaikwad, S., Bal, C. S., Chitra, S., Prasad, K., … Chandra, P. S. (2010). Intra-operative electrocorticography in lesional epilepsy. *Epilepsy Research*, *89*(1), 133–141.

Wang, W., Degenhart, A. D., Collinger, J. L., Vinjamuri, R., Sudre, G. P., Adelson, P. D., … Weber, D. J. (2009). Human motor cortical activity recorded with Micro-ECoG electrodes, during individual finger movements. In *2009 Annual International Conference of the IEEE Engineering in Medicine and Biology Society* (Vol. 2009, pp. 586–589). IEEE.

Watanabe, H., Sato, M., Suzuki, T., Nambu, A., Nishimura, Y., Kawato, M., & Isa, T. (2012). Reconstruction of movement-related intracortical activity from micro-electrocorticogram array signals in monkey primary motor cortex. *Journal of Neural Engineering*, *9*(3), 036006.

Worrell, G. a, Gardner, A. B., Stead, S. M., Hu, S., Goerss, S., Cascino, G. J., … Litt, B. (2008). High-frequency oscillations in human temporal lobe: Simultaneous microwire and clinical macroelectrode recordings. *Brain*, *131*(4), 928–937.

Zumsteg, D., & Wieser, H. G. (2000). Presurgical evaluation: current role of invasive EEG. *Epilepsia*, *41 Suppl 3*, S55–S60.

APPENDIX A

INSTITUTIONAL REVIEW BOARD DOCUMENTS

PHOENIX CHILDREN'S Hospital

September 20, 2012

P. David Adelson, MD
Phoenix Children's Hospital
Neurosurgery Department
1919 E. Thomas Road
Phoenix, AZ 85016

RE: PCH IRB #: 12-103: Spatiotemporal evolution of epileptic seizures using ECoG and EEG

Dear Dr. Adelson:

You have the permission of Phoenix Children's Hospital (PCH) to conduct the study noted above.

The research will be guided by Good Clinical Practices and conducted in accordance with all applicable Federal, State, and Local Laws and Regulations. In addition, the research will be conducted in compliance with the policies and procedures of the PCH Office of Research and the PCH Institutional Review Board (IRB).

Enclosed is the following documentation for your records:

- Scientific Review Committee approval letter
- IRB approval letter

You are required to notify the Phoenix Children's Hospital Privacy Officer or the Office of Research prior to releasing any protected health information or patient materials to third parties.

Please do not hesitate to contact the Office of Research with any questions or concerns. We look forward to the successful completion of this study.

Sincerely,

Ashley Lopez, MS
Director of Research

1919 E. Thomas Rd. • Phoenix, AZ 85016 • (602) 933-1000 • (888) 908-5437 • www.phoenixchildrens.com

PHOENIX CHILDREN'S Hospital

September 20, 2012

P. David Adelson, MD
Phoenix Children's Hospital
Neurosurgery Department
1919 E. Thomas Road
Phoenix, AZ 85016

RE: PCH IRB #: 12-103: Spatiotemporal evolution of epileptic seizures using ECoG and EEG (Expedited Review of New Study)

Dear Dr. Adelson:

I have reviewed your request for expedited approval of the new study listed above. Your study is eligible for expedited review under 21 CFR 56.110 and 45 CFR 46.110, category 5 where the research involves materials (data, documents, records, or specimens) that have been collected, or will be collected solely for non-research purposes (such as medical treatment or diagnosis).

A Waiver of Informed Consent has been granted under 45 CFR 46.116(d) (1-4).

A Waiver of HIPAA Authorization has been granted under 45 CFR 164.512(i)(1)(i)

The approval includes the following documents:

- IRB Paperwork (v.9.17.2012)
- Protocol (v.9/17/2012)
- Request for Waiver of Informed Consent (v.9/17/2012)
- Request for Waiver of HIPAA Authorization (v.9/17/2012)

The study is next subject to continuing review on or before 09/19/2013, unless closed before that date. You may not continue the study beyond the expiration date noted above. You must apply for re-approval 45 days in advance of expiration to allow adequate time for IRB review.

As Principal Investigator you are responsible for assuring that:

- The approved protocol is followed and prior IRB approval is obtained for any changes (including changes in recruitment procedures, subject, population, location, protocol); and
- Any problems are reported promptly to the IRB (including adverse events and deviations from the approved protocol).

Approval period: 09/20/2012 - 09/19/2013

If you have any questions, please contact Cherie Putnam at 602-546-0141 or cputnam@phoenixchildrens.com.

Sincerely,

Mitchell Shub, MD
Co-Chair, PCH Institutional Review Board

cc: Kari Rich
Abhinav Bharagava

PHOENIX CHILDREN'S Hospital

September 20, 2012

P. David Adelson, MD
Phoenix Children's Hospital
Neurosurgery Department
1919 E. Thomas Road
Phoenix, AZ 85016

RE: 12-103: Spatiotemporal evolution of epileptic seizures using ECoG and EEG

Dear Dr. Adelson:

Thank you for your submission of minor revisions for the above noted project. Your revisions were reviewed 09/20/2012 by the Phoenix Children's Hospital Scientific Review Committee (SRC). The SRC is a sub-committee of the Phoenix Children's Hospital Institutional Review Board (PCH IRB). SRC review and input is representative of the IRB's scientific review process.

The committee voted to recommend approval to the Medical Executive Committee and the Institutional Review Board.

Please note that the study MAY NOT be initiated until you have received the final approval letters from the IRB and the Office of Research.

If you have questions or concerns please contact Cherie Putnam at 602-546-0141, or cputnam@phoenixchildrens.com.

Sincerely,

Mitchell Shub, MD
Chair, PCH Scientific Review Committee

cc: Bhargava, Abhinav
Ashmont, Kari

September 26, 2013

P. David Adelson, MD
Phoenix Children's Hospital
Neurosurgery Department
1919 E. Thomas Road
Phoenix, AZ 85016

RE: PCH IRB #12-103: Spatiotemporal evolution of epileptic seizures using ECoG and EEG

Dear Dr. Adelson:

I have reviewed your request for continuing review of the study listed above. This study qualifies for expedited review under 21 CFR 56.110 and 45 CFR 46.110, category 5 where the research involves material (data, documents, records, or specimens) that have been collected, or will be collected solely for non-research purposes (such as medical treatment or diagnosis.)

This is to confirm that I have approved your request for continuation. You are granted permission to continue your study as described effective immediately.

This approval includes the following:

- Continuing Review Application (9/24/2013)
- Abstract: : Spatiotemporal evolution of seizures using a 3D object detection algorithm (5/9/2013)

Since your study expired on 9/20/2013, you are not permitted to use any data collected between 9/20/2013 to 9/26/2013.

The study is next subject to continuing review on or before 9/25/2014, unless closed before that date. You may not continue the study beyond the expiration date noted above. You must apply for re-approval 45 days in advance of expiration to allow adequate time for IRB review.

As Principal Investigator you are responsible for assuring that:

- The approved protocol is followed and prior IRB approval is obtained for any changes (including changes in recruitment procedures, subject, population, location, protocol); and
- Any problems are reported promptly to the IRB (including adverse events and deviations from the approved protocol).

Approval period: 09/26/2013 – 09/25/2014

If you have any questions, please contact Shy Walker at 602-546-0056; swalker@phoenixchildrens.com.

Sincerely,

Mitchell Shub, MD
Co-Chair, PCH Institutional Review Board

cc: Remy Wahnoun

September 11, 2014

P. David Adelson, MD
Phoenix Children's Hospital
Neurosurgery Department
1919 E. Thomas Road
Phoenix, AZ 85016

RE: PCH IRB #12-103: Spatiotemporal evolution of epileptic seizures using ECoG and EEG (Continuing Review)

Dear Dr. Adelson:

I have reviewed your request for continuing review of the study listed above. This study qualifies for expedited review under 21 CFR 56.110 and 45 CFR 46.110, category 5 where the research involves material (data, documents, records, or specimens) that have been collected, or will be collected solely for non-research purposes (such as medical treatment or diagnosis).

This is to confirm that I have approved your request for continuation. You are granted permission to continue your study as described effective immediately.

This approval includes the following:

- Continuing Review Application (8/27/2014)
- Abstract: Spatiotemporal Evolution of Seizures Using a 3D Object Detection Algorithm (10/17/2013)

The study is next subject to continuing review on or before 9/10/2015, unless closed before that date. You may not continue the study beyond the expiration date noted above. You must apply for re-approval 45 days in advance of expiration to allow adequate time for IRB review.

As Principal Investigator you are responsible for assuring that:

- The approved protocol is followed and prior IRB approval is obtained for any changes (including changes in recruitment procedures, subject, population, location, protocol); and
- Any problems are reported promptly to the IRB (including adverse events and deviations from the approved protocol).

Approval period: 09/11/2014 – 09/10/2015

If you have any questions, please contact Shy Walker at 602-933-0056; swalker@phoenixchildrens.com.

Sincerely,

Mitchell Shub, MD
Co-Chair, PCH Institutional Review Board

cc: Remy Wahnoun

July 2, 2015

David Adelson, MD
Phoenix Children's Hospital
BNI
1919 E. Thomas Road
Phoenix, AZ 85016

PCH IRB# 15-020: Macro and Micro Electrocorticography in Cortical Interfacing (Review of Study)

Dear Dr. Adelson:

You have the permission of Phoenix Children's Hospital (PCH) to conduct the study noted above.

The research will be guided by Good Clinical Practices and conducted in accordance with all applicable Federal, State, and Local Laws and Regulations. In addition, the research will be conducted in compliance with the policies and procedures of the PCH Office of Research and the PCH Institutional Review Board (IRB).

Enclosed is the following documentation for your records:

- IRB approval letter
- Agreement for Exchange of Research Data

You must submit all signed consents, assents, and HIPAA authorization to the Office of Research Coordinator to be uploaded into Chartmaxx.

Please do not hesitate to contact the Office of Research with any questions or concerns. We look forward to the successful completion of this study.

Sincerely,

Denise Drumm-Gurnee, PhD, M.Sc.
Director of Research Operations

cc: Danni Brown

April 9, 2015

David Adelson, MD
Phoenix Children's Hospital
BNI
1919 E. Thomas Road
Phoenix, AZ 85016

PCH IRB# 15-020: Macro and Micro Electrocorticography in Cortical Interfacing (Review of Study)

Dear Dr. Adelson:

On 4/9/2015 the modification request form dated 4/2/2015 for the above mentioned project received expedited approval by the Phoenix Children's Hospital Institutional Review Board under 21 CFR 56.110(b) (2); 45 CFR 46.110(b) (2).

This modification included revisions to incorporate the IRB required changes to the informed consent, assent, and HIPAA Authorization as requested during the fully convened meeting of the PCH IRB on 3/26/2015.

This approval includes:

- IRB Paperwork (2/26/2015)
- Informed Consent (4/2/2015)
- Assent for Children Over 8 Years of Age (4/2/2015)
- Spanish Short Form (5/31/2012)
- Authorization to Use or Disclose Protected Health Information (PHI) (2/26/2015)
- Spanish Authorization to Use or Disclose Protected Health Information (PHI) (2/26/2015)
- HIPAA Authorization to Store Protected Health Information For Future Research (4/2/2015)
- Data Collection Form
- Protocol Revision 1 (2/17/2015)

Approval period: 3/26/2015 – 3/25/2016

The study is next subject to continuing review on or before 3/25/2016, unless closed before that date. You may not continue the study beyond the expiration date noted above. You must apply for re-approval 45 days in advance of expiration to allow adequate time for IRB review.

As Principal Investigator you are responsible for assuring that:

- The approved protocol is followed and prior IRB approval is obtained for any changes (including changes in recruitment procedures, subject, population, location, protocol); and
- Any problems are reported promptly to the IRB (including adverse events and deviations from the approved protocol).

If you have any questions or require further information contact Shy Walker at 602-933-0056; swalker@phoenixchildrens.com in the IRB office.

Sincerely,

Mitchell Shub, MD
Co-Chair, PCH Institutional Review Board

cc: Danni Brown

Agreement for Exchange of Research Data

This Agreement for Exchange of Research Data ("Agreement") is between Phoenix Children's Hospital, Inc. ("Hospital), and The Arizona Board of Regents for and on behalf of Arizona State University ("Recipient").

1. Recipient wishes to review or receive certain health information which includes electrocorticography data, audio, video, photographs, electrode data, demographic and clinical information, and outcome data ("Data Set") from Hospital to perform research functions for the following research: Macro and Micro Electrocorticography in Cortical Interfacing ("Study").

2. Hospital agrees to provide access to the Data Set to Recipient to perform those research functions; and

3. Hospital and Recipient recognize this Agreement is required by the Health Insurance Portability and Accountability Act and the Standards for Privacy of Individually Identifiable Health Information, 45 C.F.R. Part 160 and Part 164, Subpart E, as amended from time to time ("Privacy Standards"), to protect the information included in the Data Set.

NOW, THEREFORE, in consideration of the mutual agreements, covenants, terms and conditions herein contained, Hospital and Recipient agree as follows:

1. Definitions. Unless otherwise provided, all capitalized terms in this Agreement will have the same meaning as provided under the Privacy Standards.

2. Uses and Disclosures of Data Set. Recipient will use and disclose the Data Set only for those purposes necessary to perform research functions in the Study, or as required by law. Recipient will not otherwise use or further disclose any information included in the Data Set.

3. Recipients Use of Subject Protected Health Information. Recipient will not use individually identifiable Study subject information or protected health information ("PHI"), and will not disclose individually identifiable Study subject information or PHI to any third party, except as permitted by the Study Protocol or unless required to do so by law, regulation, government order, or pursuant to a written request by the Study subject. This section will survive termination of this Agreement.

4. Designation of Personnel. If Recipient is not an individual person, Recipient designates the following personnel as individuals who will receive, use and disclose the Data Set on Recipient's behalf: Bradley Greger, PhD.

Recipient will require the listed personnel to comply with the terms of this Agreement. Recipient represents and warrants that the listed personnel are under legal obligation to Recipient, by contract or otherwise, to comply with Recipient's instructions to comply with this Agreement.

5. Safeguards. Recipient will implement appropriate safeguards to prevent any use or disclosure of the Data Set not otherwise permitted in this Agreement.

6. Reports of Impermissible Use of Disclosure. Recipient will report to Hospital any use or disclosure of the Data Set not permitted by this Agreement within five business days of Recipient's learning of such use or disclosure.

7. Prohibition on Identifying Information and Contracting Individuals. Recipient agrees that it will not attempt to learn the identity of the individuals who are the subject of the Data Set. If Recipient does learn the identity of the individuals, it agrees not to contact those individuals.

8. Hospital Access to Recipient Books and Records. Recipient will, within five business days' of Hospital's written request, make available during normal business hours at Recipient's offices, all records, books, agreements, policies and procedures relating to the use or disclosure of the Data Set for the purpose of allowing Hospital to determine Recipient's compliance with the Agreement.

9. Termination. Hospital immediately may terminate the Agreement upon written notice to Recipient if Hospital determines in its discretion that the Recipient has breached a material term of this Agreement. Alternatively, Hospital may elect to provide Recipient with thirty days' advance written notice of Recipient's breach of any term or condition of this Agreement, and afford Recipient the opportunity to cure the breach to the satisfaction of Hospital within twenty days of such notice. If Recipient fails to timely cure the breach, as determined by Hospital, the Agreement will terminate as provided in Hospital's notice. Within five days of termination of the Agreement, Recipient will return the Data Set to Hospital and will not keep any copies.

10. Liability. To the extent permitted by law, Recipient will defend, indemnify and hold harmless Hospital, and its officers, directors, employees and agents from and against all claims, damages, liabilities, losses, costs and expenses, including reasonable attorneys' and experts' fees and costs arising out of bodily injury of any person (including death) or property damage, but only to the extent that such claims are caused by the act, omission, negligence, misconduct or other fault of Recipient.. This section will survive termination of this Agreement.

11. Debarment and Exclusion. Recipient represents and warrants to Hospital, that Recipient and all personnel providing services to Hospital under this Agreement, as applicable, have not been placed on the sanctions list issued by the Office of the Inspector General of the Department of Health and Human Services pursuant to the provisions of 42 U.S.C. § 1320a(7), have not been excluded from government contracts by the General Services Administration ("GSA") and have not been convicted of a felony or any crime relating to healthcare. Further, if during any term of this Agreement, Recipient is placed on the sanctions list, excluded from government contracts or convicted of a felony or any crime relating to healthcare, Recipient immediately will notify Hospital in writing of the event and such notice shall contain reasonably sufficient information to allow Hospital to determine the nature of the sanction, exclusion or conviction. Hospital will have the right to terminate this Agreement immediately by written notice to Recipient if Recipient is placed on the sanctions list, banned from government contracts by GSA or convicted of a felony or any crime relating to healthcare.

12. Applicable Law. This Agreement shall be construed according to the laws of the State of Arizona, without regard to its conflicts of laws provisions.